Evaluation of six gauge-based gridded climate products for analyzing long-term historical precipitation patterns across the Lancang-Mekong River Basin ☆

Masoud Irannezhad, Junguo Liu*

School of Environmental Science and Engineering, Southern University of Science and Technology, Shenzhen 518055, China

HIGHLIGHTS

- Wetter climate across the Lancang-Mekong River Basin (LMRB) during 1981-2010.
- Wetter dry seasons and drier wet seasons across the LMRB during 1951-2010.
- Southern Oscillation Index derived wetter dry seasons in the LMRB during 1981-2010.
- Recommending GPCC/APHRODITE for precipitation analysis in the LMRB before/after 1951.

GRAPHICAL ABSTRACT
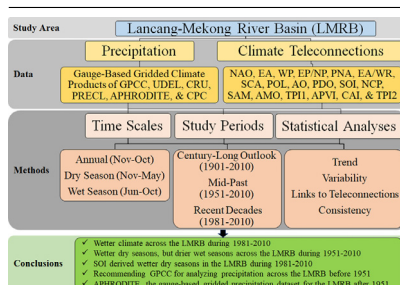
ARTICLE INFO

ABSTRACT

Freshwater plays a vital role in global sustainability by improving human lives and protecting nature. In the Lancang-Mekong River Basin (LMRB), sustainable development is principally dependent upon precipitation that predominantly controls freshwater resources availability required for both life and livelihood of ~70 million people. Hence, this study comprehensively analyzed long-term historical precipitation patterns (in terms of trends, variability, and links to climate teleconnections) throughout the LMRB as well as its upper (Lancang River Basin, LRB) and lower (Mekong River Basin, MRB) parts employing six gauge-based gridded climate products: Asian Precipitation Highly-Resolved Observational Data Integration Towards Evaluation of Water Resources (APHRODITE), Climate Prediction Center (CPC), Climate Research Unit (CRU), Global Precipitation Climatology Center (GPCC), Precipitation Reconstruction over Land (PRECL), and University of Delaware (UDEL). Accordingly, annual and seasonal (dry and wet) precipitation time series were calculated for three study periods: century-long outlook (1901-2010), mid-past (1951-2010), and recent decades (1981-2010). However, the role of climate teleconnections in precipitation variability over the LMRB was only identified during their available temporal coverages: mid-past and recent decades. The results generally showed that: (i) both annual and seasonal precipitation increased across all three basins in 1981-2010; (ii) wet and dry seasons got drier and wetter, respectively, in all basins in 1951-2010; (iii) all such changes were fundamentally attributed to increases in precipitation variability on both annual and seasonal scales over time; (iv) these variations were most strongly associated with the Pacific Decadal Oscillation (PDO), Atlantic Multi-decadal Oscillation (AMO) and East Pacific/North Pacific (EP/NP) pattern in the LMRB and the MRB during 1951-2010, but with the North Sea-Caspian Pattern (NCP) and the Southern Annular Mode (SAM) in the LRB; (v) such relationships got stronger in 1981-2010, while the Southern Oscillation Index (SOI) became the most influential teleconnection for dry season precipitation variability across all basins; and (vi) GPCC (APHRODITE) provided the most reliable gauge-based gridded precipitation time series over the LMRB for the years before (after) 1951. These findings lay a foundation for further studies focusing on water resources and sustainable development in the LMRB.

1. Introduction

According to the Sixth Assessment Report (AR6) of the Intergovernmental Panel on Climate Change (IPCC), the global surface temperature was 1.09°C warmer during 2011-2020 than 1850-1900, with a higher increase across the land (1.59°C) than over the ocean (0.88°C) (IPCC, 2021). This global warming is principally caused by increasing anthropogenic concentrations of greenhouse gas emissions to the atmosphere, with changes in the climate system of Earth (e.g., Iz, 2018; IPCC, 2021). Such unequivocal, continuing climate change has already resulted in substantial alterations in water cycle components, particularly precipitation and evapotranspiration (e.g., Berghuijs et al., 2017; Konapala et al., 2020; IPCC, 2021). Evaluating these components has been one of the main topics in international research communities for studies concentrating mainly on climatic, hydrological, and environmental changes (e.g., AghaKouchak et al., 2020; Hugelius et al., 2020; Gudmundsson et al., 2021).

Precipitation is the most important component of the hydrological cycle (Pascale et al., 2015) combining atmospheric (e.g., evaporation and cloud) and land-surface (e.g., infiltration and soil moisture) processes (e.g., Andersson et al., 2005). It is also one of the key variables for detecting climate change worldwide (e.g., Wang et al., 2018; Deininger et al., 2020; IPCC, 2021). There has likely been an increase in globally averaged precipitation across the land since 1950, with a higher rate after the 1980s (IPCC, 2021). On a regional scale, however, precipitation has considerably increased (decreased) at high (low) latitudes in recent decades (e.g., Wang et al., 2018; Deininger et al., 2020). Such changes in regional precipitation have already impacted freshwater resources (e.g., Konapala et al., 2020; IPCC, 2021; Pokhrel et al., 2021) required for improving human lives while protecting nature on Earth as the aim of the 2030 Agenda of Sustainable Development adopted by the United Nations (UN) in 2015 (UN, 2015). This is crucially important for the sustainability of regions covering developing countries, like the Lancang-Mekong River Basin (LMRB) in Mainland Southeast Asia, because of their high human population density, susceptible infrastructures, and poor land-use planning and management practices (Yin et al., 2011; Liu et al., 2017a; Irannezhad et al., 2018).

The LMRB is home to about 70 million people from six different countries of Vietnam, Thailand, Myanmar, Laos, Cambodia, and China (Zhao et al., 2021). About 40% of these inhabitants are typically living in poverty, working in basic freshwater-related sectors (e.g., agriculture, forestry, and fishery), and dependent upon different ecosystem services provided by the Lancang-Mekong River (MRC, 2019). As the primary freshwater source for this river, indeed, precipitation plays a crucial role in the sustainable economic, social, and environmental development in the LMRB (e.g., Liu et al., 2021a). Hence, improving our knowledge about historical variability and changes in precipitation across the LMRB can lead its riparian countries toward attaining water security (Sarojini et al., 2016) and consequently achieving the United Nations' Sustainable Development Goals (SDGs) (UN, 2015), particularly "No Poverty" (SDG1) and "Zero Hunger" (SDG2) (Sachs et al., 2017), on both national and regional scales (Irannezhad et al., 2022).

Applying accurate, adequate, and reliable historical datasets is critically important for a better understanding and interpretation of trends in past precipitation characteristics, in terms of intensity, frequency, and duration (e.g., Radinović and Ćurić, 2009; Chen et al., 2018; Sun et al., 2018). However, insufficient and uneven distribution of measurement stations restricts monitoring of spatio-temporal precipitation variability across the LMRB (Wang et al., 2016). Available in-situ precipitation records in this region also include discontinuities mainly due to different transboundary conflicts among all six riparian countries that follow their specific priorities and strategies for using water from the LMRB in recent decades (Lutz et al., 2014). Despite such limitations, regional and global gauge-based gridded climate datasets have basically been created applying the most reliable precipitation data collected from various sources such as measurement stations in the countries sharing the

LMRB, different groups or organizations compiling historical time series, and observations through research projects (Yatagai et al., 2009, 2012; Sun et al., 2018). Hence, such gridded time series can overcome the inhomogeneous in-situ records and improve our understanding of spatio-temporal variations and changes in precipitation across the LMRB in the past (Lutz et al., 2014). This is practically remarkable as previous studies generally reported inconsistent, inconclusive, and uncertain changes in the rate and direction of trends in historical precipitation throughout the LMRB that summarized in Liu et al. (2021a), mentioned in the supplementary material, and reviewed in the Discussion Section of this paper.

Along with analyzing regional precipitation changes, it is critically important to identify and explain their underlying complex physical and causal mechanisms. From a hydrological point of view, the spatio-temporal heterogeneity of precipitation variability throughout a region on Earth is generally related to the moisture sources and transport pathways (e.g., Liu et al., 2021b) controlled by evident patterns in different large-scale oceanic-atmospheric circulations (Pathak et al., 2017; Jiang et al., 2017; Zhu et al., 2020). The power and effect of these patterns over a certain area during a particular period of the year are generally expressed by climate teleconnection indices (hereafter, "teleconnections") (more information in the supplementary material); e.g., the North Atlantic Oscillation (NAO). Numerous studies have described the main components of these teleconnections (e.g., Glantz et al., 2009) and their linkages to historical variations in precipitation on different parts of Earth (e.g., Irannezhad et al., 2014; Chen et al., 2019; Yang et al., 2019; Hrudya et al., 2021; Ghasemifar et al., 2022). A better understanding of significant associations between regional precipitation variability and teleconnections can lead to developing climate change mitigation and adaptation strategies (IPCC, 2021), with a focus on hydrological forecasting, water security, and global sustainability (Jiang et al., 2012; Liu et al., 2017b; Irannezhad et al., 2022). For the LMRB, however, previous studies have mostly measured the correlations of a few teleconnections with precipitation time series only extracted from one of the available gauge-based gridded precipitation products (e.g., Chen et al., 2019; Irannezhad et al., 2020, 2021).

Using the existing regional and global gauge-based gridded climate products, the overall aim of this study is to provide a comprehensive assessment of historical precipitation patterns over the LMRB. The specific objectives are to: (1) test whether there is a change in precipitation across the LMRB over time; (2) analyze spatio-temporal variations in precipitation throughout this basin; (3) measure relationships of such regional precipitation variability with different influential teleconnections; and (4) investigate the consistencies among different gauge-based gridded precipitation datasets over the LMRB. The results lay a foundation for employing gauge-based gridded climate products in further studies focusing particularly on both SDG1 ("No Poverty") and SDG2 ("Zero Hunger") in the LMRB by integrating meteorological, hydrological, agricultural, and socio-economic processes into an interdisciplinary "web" model (Liu et al., 2019).

2. Materials and methods

2.1. Study area

The Lancang-Mekong (LM) River in Mainland Southeast Asia (Fig. 1a), with a drainage basin area of about 795 10^3 km^2, is one of the largest rivers around the world in terms of mean annual discharge (475 10^3 m^3) (Gupta et al., 2002; Jacobs, 2002; MRC, 2010). It originates throughout the Tibetan Plateau in China and runs through Myanmar, Laos, Thailand, and Cambodia before entering the Mekong Delta in Vietnam and then releasing to the South China Sea. Hence, the LMRB has a high population density of 85.2 people km^{-2}, which is expected to promptly intensify in the future (MRC, 2019; Zhao et al., 2021). In general, the LMRB is geographically divided into two parts: the upper (Lancang River Basin, LRB) and lower (Mekong River Basin, MRB) (Fig. 1b).
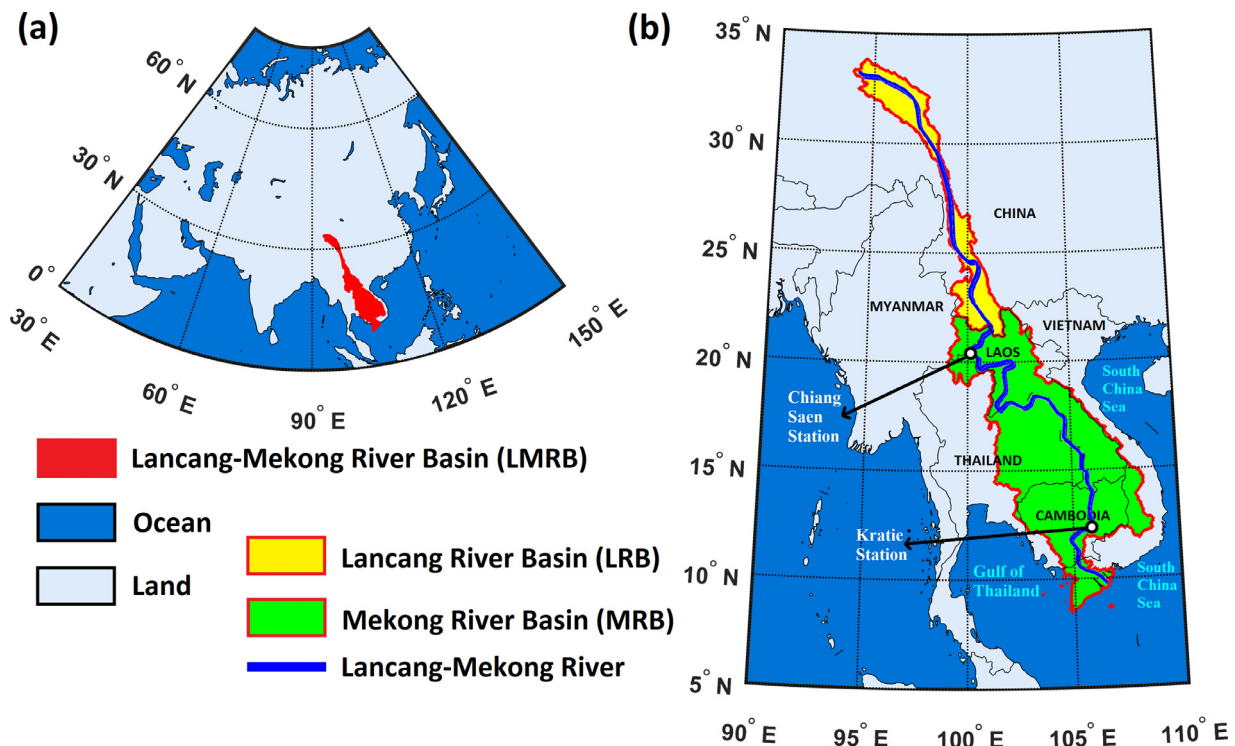
Fig. 1. (a) The location of the Lancang-Mekong River Basin (LMRB) and (b) the Lancang River Basin (LRB) and the Mekong River Basin (MRB).

The division point is located at the Chiang Saen discharge measurement station in the most northern part of Thailand, close to its bored with China (Fig. 1b). In the LRB with a length of 2000 km, from its headwaters to the Chiang Saen station, the elevation sharply (2 m km^{-1}) falls from 4500 m to about 500 m (MRC, 2005). However, between the Chiang Saen and the Kratie discharge measurement stations throughout the MRB (Fig. 1b), the river experiences a moderately steep slope (0.25 m km^{-1}) over a distance of 2000 km, meaning a decline in elevation from 500 m to a few tens of meters (MRC 2005). In the downstream, from the Kratie station on the Mekong Delta through the South China Sea (~600 km), the river bed experiences a steep slope of 0.03 (m km^{-1}) (MRC, 2005). Accordingly, the LMRB area consists of (i) the LRB (24%), including the contributions of China (21%) as well as Myanmar (3%), and (ii) the MRB (76%), comprising the shares 25% from Laos, 23% from Thailand, 20% from Cambodia, and 8% from Vietnam (MRC, 2005).

The Indian Summer Monsoon (ISM), the East Asian Monsoon (EAM), Tropical Cyclones (TCs), and the El Niño-Southern Oscillation (ENSO) naturally influence precipitation variability across the LMRB (MRC, 2010; Delgado et al., 2012; Räsänen and Kummu, 2013). Interannual variations in precipitation over the LMRB are principally governed by the ENSO, which regulates the variability of Asian monsoon including the ISM and the Western North Pacific Monsoon (WNPM) (Ward et al., 2010; Räsänen and Kummu, 2013). Accordingly, annual precipitation is primarily shared between the wet (Jun-Oct) and dry (Nov-May) seasons, by 70% and 30%, respectively. In general, the ISM conveys extensive atmospheric water vapor content from the Indian Ocean to the LMRB, particularly arriving from the southwest and partially from the southeast, during the wet season. The TCs also contribute to extreme precipitation events (Chen et al., 2019) during the wet season, mainly its last three months (Aug-Oct). During the dry season, however, the EAM induces a high pressure across the LMRB. Thus, non-stationary atmospheric circulations in response to climate change can explain alterations in hydrometeorology over the LMRB (Delgado et al., 2010).

2.2. Data description

2.2.1. Gauge-based gridded climate products

In-situ precipitation observations are basically collected by national weather services. Integrating all such observations from different nations into one common global dataset has always been essential for climatology, hydrology, water resources, and geophysics. Hence, the World Meteorological Organization was established in 1873 as an intergovernmental organization including 191 members (http://www.wmo.int) for developing and standardizing in-situ observations on Earth. In 1992, the Global Climate Observing System (GCOS) was founded to make the climate-related data, from local to global scale (Houghton et al., 2012), freely available to all countries (Spence and Townshend, 1995). Based on different counting criteria (Kidd et al., 2017), the total number of worldwide precipitation measurement stations ranges between 150,000 and 250,000, although not all have contemporarily or constantly operated (Groisman and Legates, 1995; New et al., 2001; Strangeways, 2006). Irregular distribution of these stations around the world motivated generating different gridded precipitation datasets for various climate-related research purposes and applications. Hence, several global and regional gridded climate products at different spatial resolutions have been produced based entirely on the in-situ precipitation records (e.g., Sun et al., 2018; Yatagai et al., 2009, 2012). This paper extracted monthly precipitation time series for the LMRB from these gauge-based gridded climate products, which are summarized in Table 1 and briefly described in the supplementary material.

2.2.2. Teleconnections

To describe the oceanic-atmospheric circulation patterns, this study considered 18 teleconnections (Table 2) based on previous studies. The monthly values of these teleconnections were obtained from different sources, covering the years since 1951. The present paper calculated the

Table 1
Summary of six global and regional gauge-based gridded climate products generated using in-situ precipitation records.

Coverage	Product	Resolution	Frequency	Study period	Source	Reference
Global land	GPCC	$0.5° \times 0.5°$	Monthly	1901-2010	GPCC	(Rudolf et al., 2009; Schneider et al., 2014)
	UDEL		Monthly	1901-2010	University of Delaware	(Willmott and Matsuura, 1995)
	CRU		Monthly	1901-2010	The CRU (University of East Anglia)	(Harris et al., 2014b; New et al., 2000)
	PRECL		Monthly	1951-2010	NCEP/NOAA	(Chen et al., 2002)
	CPC		Daily	1981-2010	CPC	(Xie et al., 2010)
Asia	APHRODITE	$0.5° \times 0.5°$	Daily	1951-2010	Japan Meteorological Agency	(Yatagai et al., 2009, 2012)

Table 2
Summary of teleconnections considered in this study.

ID	Climate teleconnection	Source	Reference
AMO	Atlantic Multi-decadal Oscillation	PSD	(Enfield et al., 2001)
AO	Arctic Oscillation	CPC	(Thompson and Wallace, 1998)
APVI	Asian Polar Vortex Index	NCC	(NCC, 2019)
CAI	Cold Air Index	NCC	(NCC, 2019)
EA	East Atlantic	CPC	(Barnston and Livezey, 1987)
EA/WR	East Atlantic/West Russia	CPC	(Barnston and Livezey, 1987; Lim and Kim, 2013)
EP/NP	Eat Pacific/North Pacific	CPC	(Barnston and Livezey, 1987)
NAO	North Atlantic Oscillation	CPC	(Barnston and Livezey, 1987)
NCP	North Sea-Caspian Pattern	CRU	(Kutiel and Benaroch, 2002)
PDO	Pacific Decadal Oscillation	NCAR	(Zhang and Levitus, 1997)
PNA	Pacific North American	CPC	(Barnston and Livezey, 1987)
POL	Polar/Eurasia pattern	CPC	(Barnston and Livezey, 1987)
SAM (AAO)	Southern Annular Mode (Antarctic Oscillation)	NCAR (CPC)	(Marshall, 2003)
SCA	Scandinavia pattern	CPC	(Barnston and Livezey, 1987; Bueh and Nakamura, 2007)
SOI	Southern Oscillation Index	NCAR	(Trenberth, 1984)
TPI1	Trans Polar Index	CRU	(Jones et al., 1999)
TPI2	Tibetan Plateau Index	NCC	(NCC, 2019)
WP	West Pacific	CPC	(Wallace and Gutzler, 1981)

average of such monthly values for the period Jan-Dec, Jun-Oct, and Nov-May as the corresponding teleconnection time series for annual scale, wet and dry seasons, respectively, for both periods of 1951-2010 and 1981-2010. The Asian Polar Vortex Index (APVI), the Cold Air Index (CAI), and the Tibetan Plateau Index (TPI) were particularly drawn from a set of 74 indices issued by the National Climate Center (NCC) of the China Meteorological Administration (CMA). The main characteristics and time series of all 18 teleconnections can be found in references and data sources, respectively, given in Table 2.

2.3. Statistical methods

In general, the Mann-Kendall (MK) non-parametric test (Mann, 1945) is applied for detecting statistically significant ($p<0.05$) trends in precipitation time series. The Sen's method (Sen, 1968) is normally used to estimate the slope of such significant trends. Instead of the Pearson's correlation coefficient (r), the Spearman's rank correlation (ρ) is preferably utilized to quantify the spatio-temporal consistency among different global and regional gauge-based gridded precipitation datasets, and also their relationships with teleconnections. This is mainly referred to the fact that the ρ, unlike the r, assumes no normality or other special distribution functions for variables (Helsel and Hirsch, 1992). In the existence of positive autocorrelation in precipitation time series, however, the trend-free pre-whitening (TFPW) method (Yue et al., 2002) for determining significant trends and the residual bootstrap (RB) approach (Park and Lee, 2001) with 5000 independent replications for examining the standard deviation of the Spearman's rank correlations (ρ) are recommended. This paper employed such statistical methods to investigate historical precipitation patterns over the LMRB based on six different global/regional gauge-based gridded ($0.5° \times 0.5°$) climate products of APHRODITE, CPC, CRU, GPCC, PRECL, and UDEL (Table 1). The monthly precipitation datasets for the CPC and APHRODITE products were calculated based on their daily records. For all precipitation datasets and teleconnections, then,

annual (Jan-Dec), wet (Jun-Oct) and dry (Nov-May) seasons time series were computed using their monthly data.

3. Results

3.1. Historical precipitation changes across the LMRB

3.1.1. Century-long outlook (1901-2010) of wetting and drying trends

A statistically significant ($p<0.05$) wetting trend (0.73 mm yr^{-1}) in annual precipitation was found for CRU dataset over the LMRB during 1901-2010, while UDEL showed a significant drying trend at the rate of 1.56 mm yr^{-1} (Fig. 2a). Similarly, significant wetting (0.83 mm yr^{-1}) and drying (-1.28 mm yr^{-1}) trends in annual precipitation were determined for CRU and UDEL datasets, respectively, over the MRB in 1901-2010 (Fig. 2a). Such century-long decreases in the UDEL annual precipitation were mainly seen over the south and southeast parts of the MRB (Fig. 2c), while the increases in the CRU across the north-eastern areas of the MRB (Fig. 2d). The UDEL dataset also showed a significant drying trend (-0.67 mm yr^{-1}) in annual precipitation over the entire LRB during 1901-2010 (Fig. 2a). Such a drying trend was mainly attributed to significant decreases in annual precipitation over the northern parts of LRB (Fig. 2c).

The LMRB experienced a drying trend (-1.13 mm yr^{-1}, $p<0.05$) in the wet season during 1901-2010 based on the UDEL datasets (Fig. 2e). This dataset also showed such drier wet seasons over the MRB during the last century, but GPCC and CRU datasets determined significant wetting trends of 0.44 and 0.63 mm yr^{-1}, respectively, in wet season precipitation (Fig. 2e). Wet seasons became wetter mainly across the northeastern parts of the MRB based on the GPCC (Fig. 2f) and CRU (Fig. 2h) datasets, but drier over the southern areas according to the UDEL product (Fig. 2g). For the LRB, all GPCC, UDEL, and CRU products determined drying trends in wet seasons precipitation over the northern parts during 1901-2010 (Fig. 2f-h).

The dry season got drier over the LMRB, LRB, and MRB during 1901-2010 based only on the UDEL product, at the rates of 0.58, 0.39, and
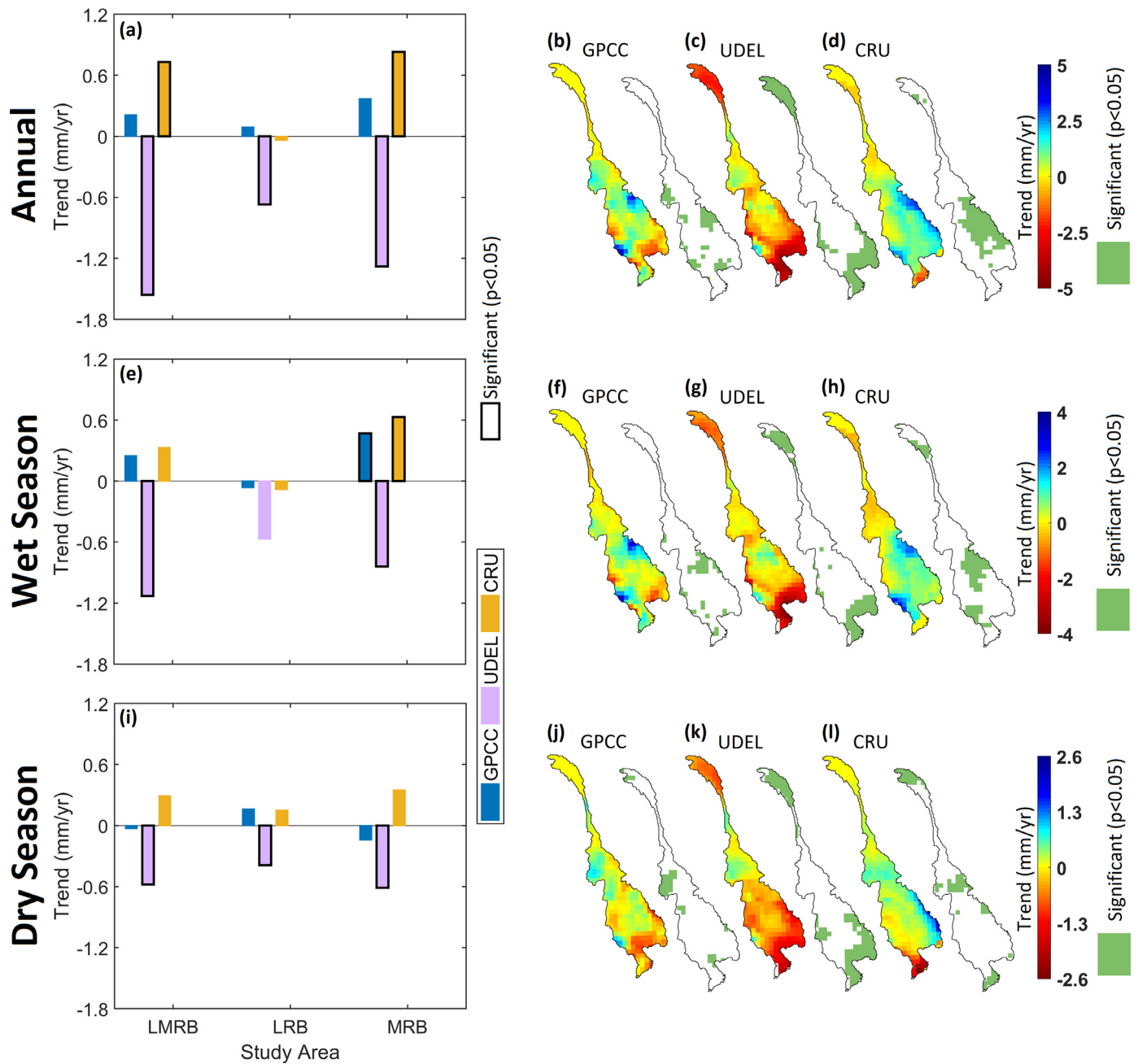
Fig. 2. Trends in annual (a-d) and seasonal (e-l) precipitation over the LMRB, LRB, and MRB during 1901-2010 based on the GPCC, UDEL, and CRU products.

0.61 (mm yr^{-1}), respectively (Fig. 2i). Such drier dry seasons were mainly found over the south and southeast of the MRB as well as the northern parts of LRB (Fig. 2k). The LMRB, LRB, and MRB experienced no clear century-long changes in dry season precipitation based on the GPCC and the CRU (Fig. 2i), although these products showed wetter dry seasons predominantly over the north of the MRB (Fig. 2j and Fig. 2l).

3.1.2. Mid-past (1951-2010) climate: wetter or drier?

APHRODITE is the only product showing significant wetting trends in annual precipitation over both LMRB and MRB during 1951-2010 (Fig. 3a). Across the LRB, all six gauge-based gridded climate products determined increases in annual precipitation (ranging 0.24-0.81 mm yr^{-1}) over 1951-2010, but all were statistically insignificant (Fig. 3a). During 1951-2010, spatial trend analysis found significant increases in

annual precipitation largely across the north and southeast of the MRB based on the APHRODITE product (Fig. 3f). However, all six gauge-based gridded climate products determined significant drying trends in annual precipitation throughout the west of the MRB over 1951-2010 (Fig. 3b-f).

For the wet season, the APHRODITE showed a significant increasing trend (0.69 mm yr^{-1}) over the LMRB during 1951-2010, but the UDEL product showed a significant decreasing trend of -1.14 mm yr^{-1} (Fig. 3g). Similarly, significant wetting (1.50 mm yr^{-1}) and drying (-2.11 mm yr^{-1}) trends in annual precipitation over the MRB during 1951-2010 were found according to the APHRODITE and the UDEL products, respectively (Fig. 3g). The wet season showed statistically significant drying trends across the western and northern parts of the MRB as well as the southern areas of the LRB during 1951-2010 (Fig. 3h-l). How-
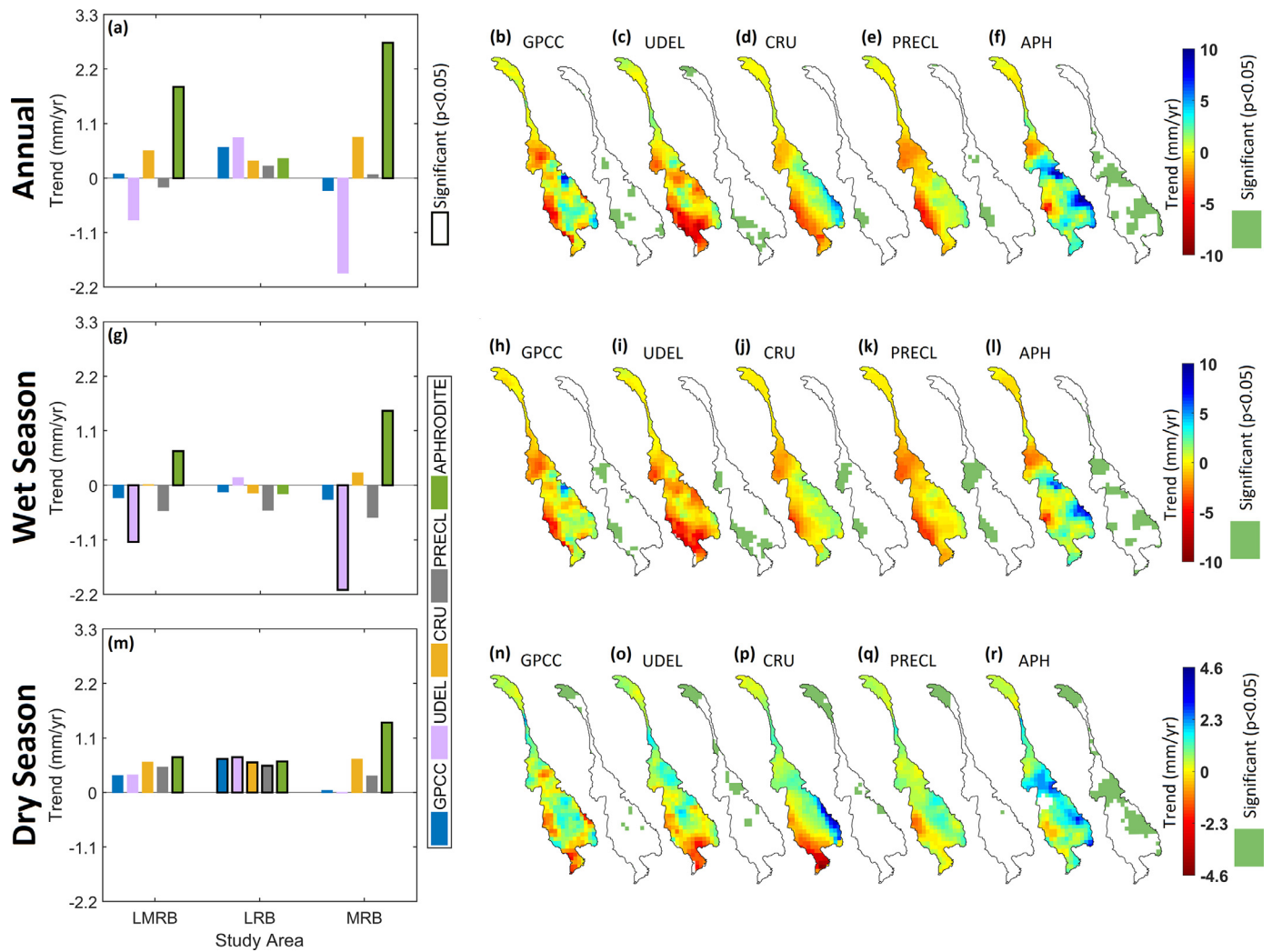
Fig. 3. Trends in annual (a-f) and seasonal (g-r) precipitation over the LMRB, LRB, and MRB during 1951-2010 based on the GPCC, UDEL, CRU, PRECL, and APHRODITE (APH) products.

ever, wetter wet seasons were occasionally seen over the east of the MRB based on the APHRODITE dataset (Fig. 3l).

On basin scale, all five gauge-based gridded climate products generally determined wetting trends in dry season precipitation over the LMRB, LRB, and MRB during 1951-2010 (Fig. 3m). Such wetting trends were all statistically significant over the LRB based on all these five products, while across the LMRB and MRB based only on the APHRODITE (Fig. 3m). Statistically significant increases in dry season precipitation were predominantly observed throughout the northern parts of the LRB during 1951-2010 (Fig. 3n-r). The APHRODITE was the only product that also showed significant wetting trends in dry season precipitation over the north and southeast of the MRB (Fig. 3r).

3.1.3. More or less precipitation in recent decades (1981-2010)

In recent decades (1981-2010), annual precipitation generally increased over the LMRB, LRB, and MRB (Fig. 4a). Such increases were statistically significant over the LMRB based on the UDEL and the APHRODITE, and over the MRB according to the UDEL, the PRECL, and the APHRODITE (Fig. 4a). However, no gauge-based gridded precipitation product found significant trends in annual precipitation over the LRB during 1981-2010 (Fig. 4a). On the spatial scale, significant decreases in annual precipitation were mainly observed across the east and southeast of the MRB determined by all six gauge-based gridded

climate products (Fig. 4b-g). However, only the APHRODITE (Fig. 4f) and the CPC (Fig. 4g) products identified increases in annual precipitation over the southeast and north of the MRB in the last climatological period (1981-2010).

Except for the CPC, all other gauge-based gridded climate products determined wetter wet seasons over the LMRB, LRB, and MRB in recent decades (Fig. 4h). However, the only significant increasing trend (3.33 mm yr^{-1}) in wet season precipitation was determined by the APHRODITE for the MRB during 1981-2010 (Fig. 4h). For wet season precipitation, the CPC was the only product showing decreases across all LMRB, LRB, and MRB over 1981-2010, but statistically insignificant (Fig. 4n). However, such drying trends in wet season precipitation were significant over the southeast and north of the MRB (Fig. 4n).

In general, the dry season became wetter over the LMRB, LRB, and MRB during 1981-2010 (Fig. 4o). Such wetting trends in dry season precipitation were statistically significant over the LMRB and MRB, based only on the APHRODITE dataset (Fig. 4o). On the spatial scale, significant increases in dry season precipitation were mostly seen across the south of the MRB as well as the north of the LRB (Fig. 4p-u). On the other hand, significant drying trends in dry season precipitation were occasionally observed over the northern parts of the MRB that were only found by the CPC product (Fig. 4u).
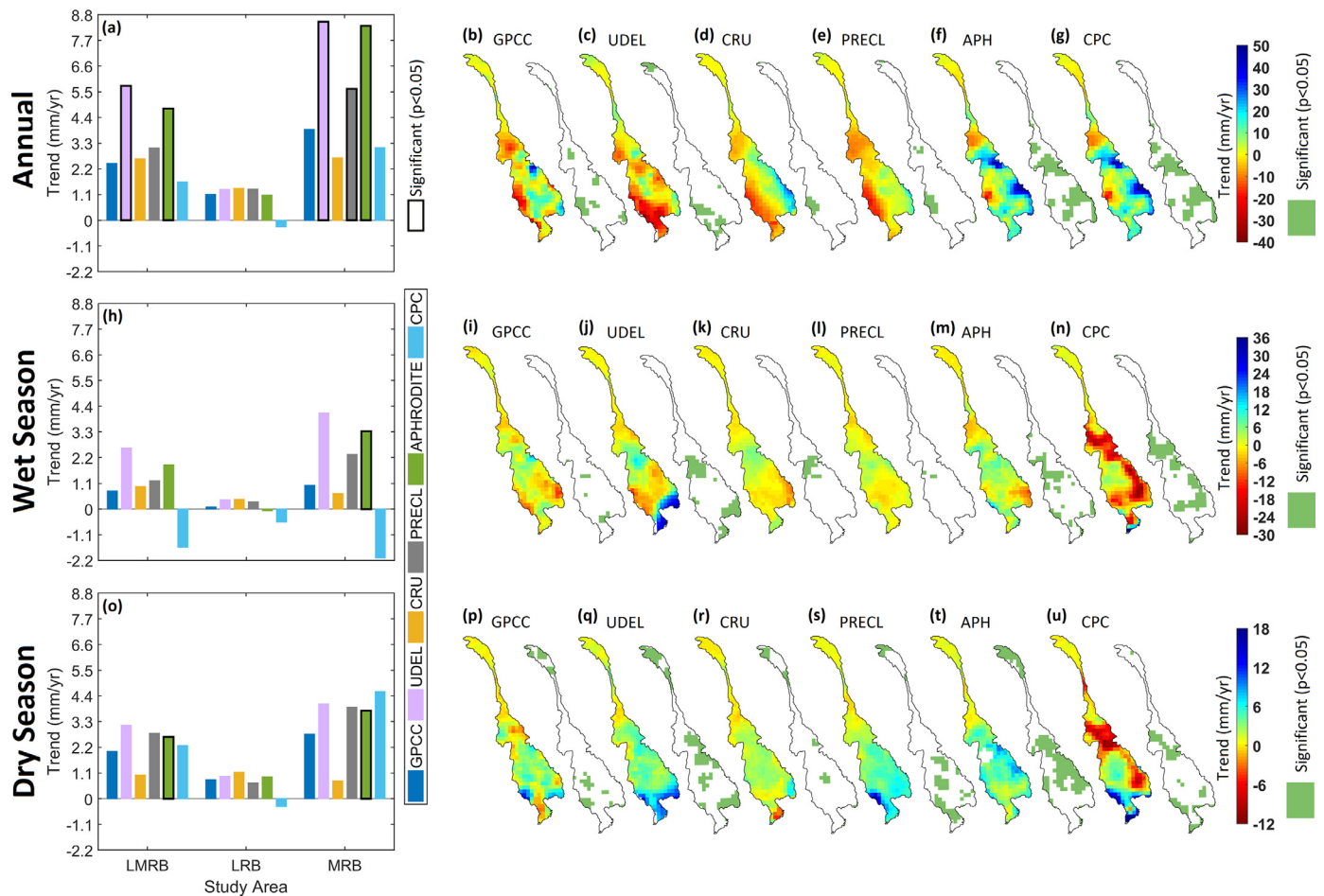
Fig. 4. Trends in annual (a-g) and seasonal (h-u) precipitation over the LMRB, LRB, and MRB during 1981-2010 for the GPCC, UDEL, CRU, PRECL, APHRODITE (APH), and CPC products.

3.2. Spatio-temporal precipitation variability throughout the LMRB

3.2.1. Annual scale

Long-term (1901-2010) average values for annual precipitation were 1337.6 mm (CRU), 1434.9 mm (GPCC), and 1471.7 mm (UDEL) across the LMRB (Fig. 5a). During 1901-2010, annual precipitation over the LMRB ranged from 1126.7 mm in 1936 (CRU) to 1754.5 mm in 1904 (UDEL) (Fig. 5a). Through the mid-past period (1951-2010), long-term average values of annual precipitation over the LMRB ranged between 1152.6 mm (APHRODITE) and 1273.8 mm (GPCC) (Fig. 5b), which was less than the range during 1901-2010. The minimum and maximum annual precipitation amounts over the LMRB were 1010.8 mm in 1958 (APHRODITE) and 1679.6 mm in 1977 (GPCC) (Fig. 5b), which exceeded the range of the same variability during 1901-2010. In recent decades (1981-2010), the long-term average values of annual precipitation over the LMRB varied from 1143.3 mm (CPC) to 1444.8 mm (GPCC), while the highest and lowest annual precipitation amounts were 898.3 mm in 1982 (CPC) and 1679.6 mm in 1999 (GPCC), respectively (Fig. 5b). Such ranges in the annual precipitation over the LMRB during 1981-2010 was greater than during 1951-2010. In general, annual precipitation showed higher ranges of historical variability across the LMRB over time. The highest values of annual precipitation across the LMRB were predominantly found in 1999 throughout all three study periods (Fig. 5a-c). However, the lowest annual precipitation was generally recognized in 1936 during 1901-2010 (Fig. 5a), but in 1992 during both 1951-2010 and 1981-2010 periods (Fig. 5b and c). Besides, spatial scale assessment identified the lowest long-term average values of annual precipitation (~200 mm) over the most northern parts of the LRB, but the highest ones (~4700 mm) mainly over the southeast, southwest, and northeast of the MRB (Fig. 6a-c).

Over the LRB, long-term average values of annual precipitation ranged between 765.4 mm (CRU) and 973.5 mm (UDEL) for 1901-2010 (Fig. 5a), 747.5 mm (APHRODITE) and 914.5 mm (UDEL) for 1951-2010 (Fig. 5b), and 745.6 mm (CPC) and 924.1 mm (UDEL) for 1981-2010 (Fig. 5c). The lowest and highest annual precipitation values over the LRB were 592.1 mm in 1906 (CRU) and 985.5 mm in 1918 (GPCC) for 1901-2010 (Fig. 5a), 647.6 mm in 1953 (APHRODITE) and 1018.7 mm in 2001 (UDEL) for 1951-2010 (Fig. 5b), and 571.1 mm in 1994 (CPC) and 1018.7 mm in 2001 (UDEL) for 1981-2010 (Fig. 5c), respectively. Both CRU and GPCC identified 1906 and 1918 as the corresponding years to the minimum and maximum annual precipitation over the LRB during 1901-2010 (Fig. 5a). However, 1992 and 2001 are generally corresponding years for both periods of 1951-2010 and 1981-2010 (Fig. 5b and c). Across the LRB, annual precipitation spatially decreased from north to south (Fig. 6a-c).

Long-term average values of annual precipitation over the MRB varied from 1679.7 mm (CRU) to 1777.3 mm (GPCC) during 1901-2010 (Fig. 5a), from 1383.1 mm (APHRODITE) to 1788.6 mm (GPCC) during 1951-2010 (Fig. 5b), and from 1376.9 mm (CPC) to 1789.3 mm (GPCC) during 1981-2010 (Fig. 5c). The highest annual precipitation across the MRB was about 2164.4 mm in 1904 determined by the UDEL, while the lowest was 985.6 mm in 1999 found in the CPC dataset (Fig. 5a-c). The minimum (maximum) annual precipitation over the MRB was generally corresponding to the years 1992-1993 (1999-2000). Spatially, the
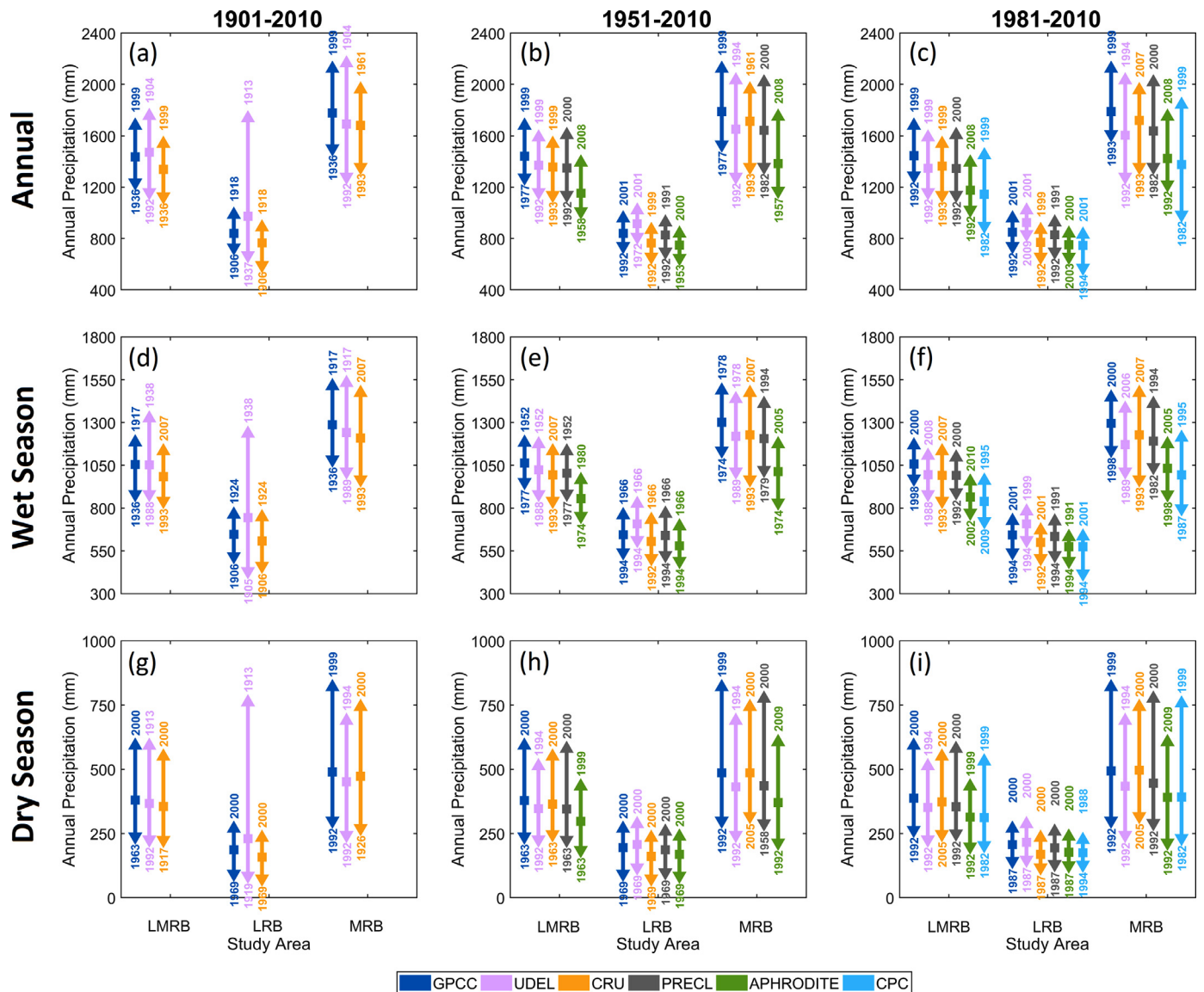
Fig. 5. Variations in annual (a-c) and seasonal (d-i) precipitation over the LMRB, LRB, and MRB during 1901-2010, 1951-2010, and 1981-2010 based on all six gauge-based gridded climate products of GPCC, UDEL, CRU, PRECL, APHRODITE (APH), and CPC.

highest long-term values of annual precipitation were observed over the southeast and northeast of the MRB (Fig. 6a-c).

3.2.2. Wet and dry seasons

Across the LMRB, long-term average values for wet season precipitation ranged between 983.5 mm (CRU) and 1054.8 mm (GPCC) during 1901-2010 (Fig. 5d), 855.1 mm (APHRODITE) and 1062.5 mm (GPCC) during 1951-2010 (Fig. 5e), and 838.1 mm (CPC) and 1056.7 mm (GPCC) during 1981-2010 (Fig. 5f). Such long-term values for wet season precipitation over the LRB (MRB) were 607.9-743.8 mm (1207.8-1287.1 mm) in 1901-2010 (Fig. 5d), 579.1-707.3 mm (1012.4-1301.1 mm) in 1951-2010 (Fig. 5e), and 573.3-708.1 mm (993.8-1294.3 mm) in 1981-2010 (Fig. 5f). The highest value of wet season precipitation was from 722.6 mm in 2009 (CPC) to 880.9 mm in 1988 (UDEL) across the LMRB, while the lowest was between 1166.7 mm in 2000 (GPCC) and 1324.1 mm in 1938 (UDEL) (Fig. 5d-f). These minimum and maximum values for wet season precipitation were 416.8 mm in 1994 (CPC) and 1235.1 mm in 1938 (UDEL) in the LRB, while 798.1 mm in 1987 (CPC) and 1531.1 mm in 1917 (UDEL) across the MRB, respectively (Fig. 5d-f). In general, the LRB experienced the lowest (highest) wet season precip-

itation in 1906 (1924) over the period 1901-2010 (Fig. 5d), but in 1994 (1966) through the years after 1951 (Fig. 5e). However, such agreement in the years of minimum and maximum values for wet season precipitation was not found over the LMRB and the MRB. Spatially, the low values of wet season precipitation were observed over the northern parts of the LRB, but the high ones over the southwest and northeast of the MRB (Fig. 6d-f).

For dry season precipitation, long-term average values over the LMRB ranged from 354.6 mm (CRU) to 380.1 mm (GPCC) for 1901-2010 (Fig. 5g), from 297.6 mm (APHRODITE) to 378.4 mm (GPCC) for 1951-2010 (Fig. 5h), and from 311.5 mm (CPC) to 387.1 mm (GPCC) for 181-2010 (Fig. 5i). These long-term values of dry season precipitation over the LRB (MRB) were 157.6-229.9 mm (451.2-489.9 mm) in 1901-2010 (Fig. 5g), 160.6-207.5 mm (370.1-486.4 mm) in 1951-2010 (Fig. 5h), and 169.1-215.3 mm (391.1-496.1 mm) in 1981-2010 (Fig. 5i). The minimum value of dry season precipitation was from 185.1 mm in 1963 (APHRODITE) to 224.3 mm in 1917 (CRU) across the LMRB, while the maximum was about 592.5 mm in 2000 (GPCC) (Fig. 5g-i). The lowest and highest values for dry season precipitation were 74.1 mm in 1969 (CRU) and 761.1 mm in 1913 (UDEL) in the
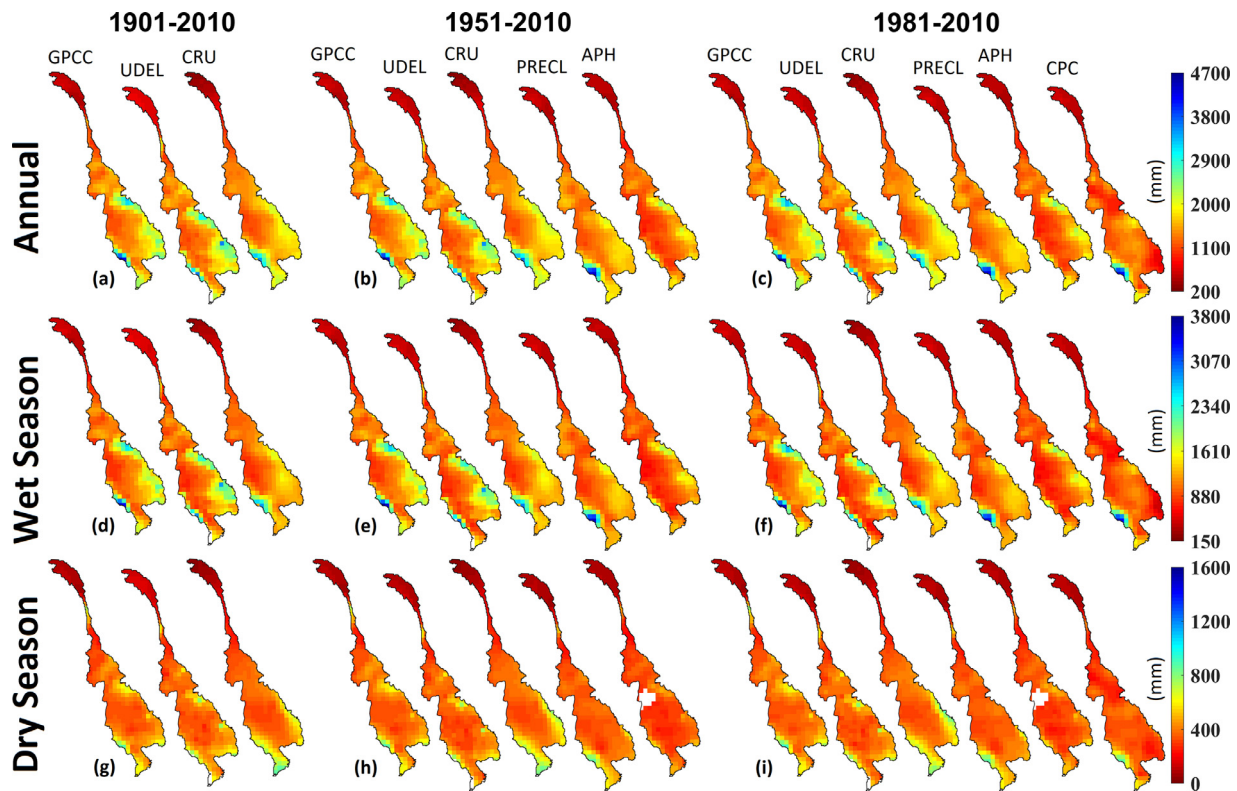
Fig. 6. Spatio-temporal variations in historical long-term average values for annual (a-c) and seasonal (d-i) precipitation throughout the LMRB during 1901-2010, 1951-2010, and 1981-2010 based on all six gauge-based gridded climate products of GPCC, UDEL, CRU, PRECL, APHRODITE (APH), and CPC.

LRB, while 213.8 mm in 1992 (APHRODITE) and 819.9 mm in 1999 (GPCC), respectively (Fig. 5g-i). The LMRB and the LRB generally experienced the lowest wet season precipitation in 1963 and 1969 during 1951-2010, respectively (Fig. 5h), while in 1992 and 1987 through the years after 1981 (Fig. 5i). For both of these basins, the highest dry season precipitation was commonly found in 2000 during all three study periods (Fig. 5g-i). Besides, the dry seasons were naturally wetter over the northeast and southwest of MRB than over the northern areas of LRB (Fig. 6g-i).

3.3. Relationships of precipitation with teleconnections over the LMRB

On basin scale, annual precipitation was significantly correlated with PDO (ρ = -0.25 to -0.49), EP/NP (ρ = -0.26 to -0.40) and AMO (ρ = 0.26 to 0.42) over both the LRMB and the MRB during 1951-2010, while with NCP (ρ = -0.29 to -0.30) and SAM (ρ = 0.27 to 0.30) across the LRB (Fig. 7a-c). In general, these relationships were stronger during 1981-2010, particularly with PDO (ρ = -0.35 to -0.57) and AMO (ρ = 0.28 to 0.53) in all three basins, with EP/NP (ρ = -0.34 to -0.63) and SOI (ρ = 0.34 to 0.52) over the LMRB and the MRB, and with SAM (ρ = 0.36 to 0.45) over the LRB (Fig. 7d-f). Such differences between 1951-2010 and 1981-2010 were also observed on the spatial scale of the LRB (Fig. 8). The strongest correlations of annual precipitation with SAM over the north of LRB during 1951-2010 (Fig. 8a-e) were generally associated with TPI1 in 1981-2010 (Fig. 8f-k). However, annual precipitation was most significantly associated with AMO over the most northern parts of the LRB during both study periods (Fig. 8). In the west of MRB, the strongest relationships were largely found between annual precipitation and TPI1 during 1951-2010 (Fig. 8a-e), while not in 1981-2010 (Fig. 8f-k). Spatial analysis of correlations between teleconnections and annual precipitation from different gauge-based gridded climate products identified no common patterns over the

west, north, and south of the MRB during 1951-2010 and 1981-2010 (Fig. 8).

Wet season precipitation was most significantly associated with PDO (ρ = -0.31 to -0.41) over the LMRB and the MRB during 1951-2010 (Fig. 9a and c), but with NCP (ρ = -0.29 to -0.37) across the LRB (Fig. 9b). In recent decades (1981-2010), however, the strongest correlations of wet season precipitation over the LRB and the MRB were generally measured with SAM (ρ = 0.35 to 0.49) and AO (ρ = 0.40 to 0.56), respectively (Fig. 9e and f). In northern parts of the LRB, wet season precipitation largely showed the strongest relationships with SAM during 1951-2010 (Fig. 10a-e), but with AMO in 1981-2010 (Fig. 10f-k). The highest correlations of wet season precipitation over the north and southeast of MRB were with SOI and NCP, respectively, through the year 1951-2010 (Fig. 10a-e). Wet season precipitation across the southeast of MRB was strongly connected to PNA in 1981-2010 (Fig. 10f-k). No other mutual spatial pattern in relationships between wet season precipitation and teleconnections was identified over the other areas of the LMRB.

Dry season precipitation showed the highest correlations with SOI over the LMRB and MRB (ρ = 0.28 to 0.47) during 1951-2010, (Fig. 11a and c). Such relationships were generally stronger (ρ = 0.42 to 0.76) in 1981-2010 (Fig. 11d and f). Across the LRB, dry season precipitation was most significantly associated with APVI (ρ = -0.27 to -0.36) through 1951-2010 (Fig. 11b), but with AMO (ρ = 0.37 to 0.45) during 1981-2010 (Fig. 11b). Spatially, the strongest relationships of dry season precipitation over the most northern parts of LRB were found with AMO in 1951-2010, across northern and central LRB with CAI, and throughout the south of LRB with AO (Fig. 12a-e). Besides, NCP was the most powerful teleconnection affecting variations in dry season precipitation over the south, east, and west of the MRB (Fig. 12a-e). During 1981-2010, however, dry season precipitation was most strongly correlated with SOI over the entire MRB, and even some parts of northern LRB (Fig. 12f-k).
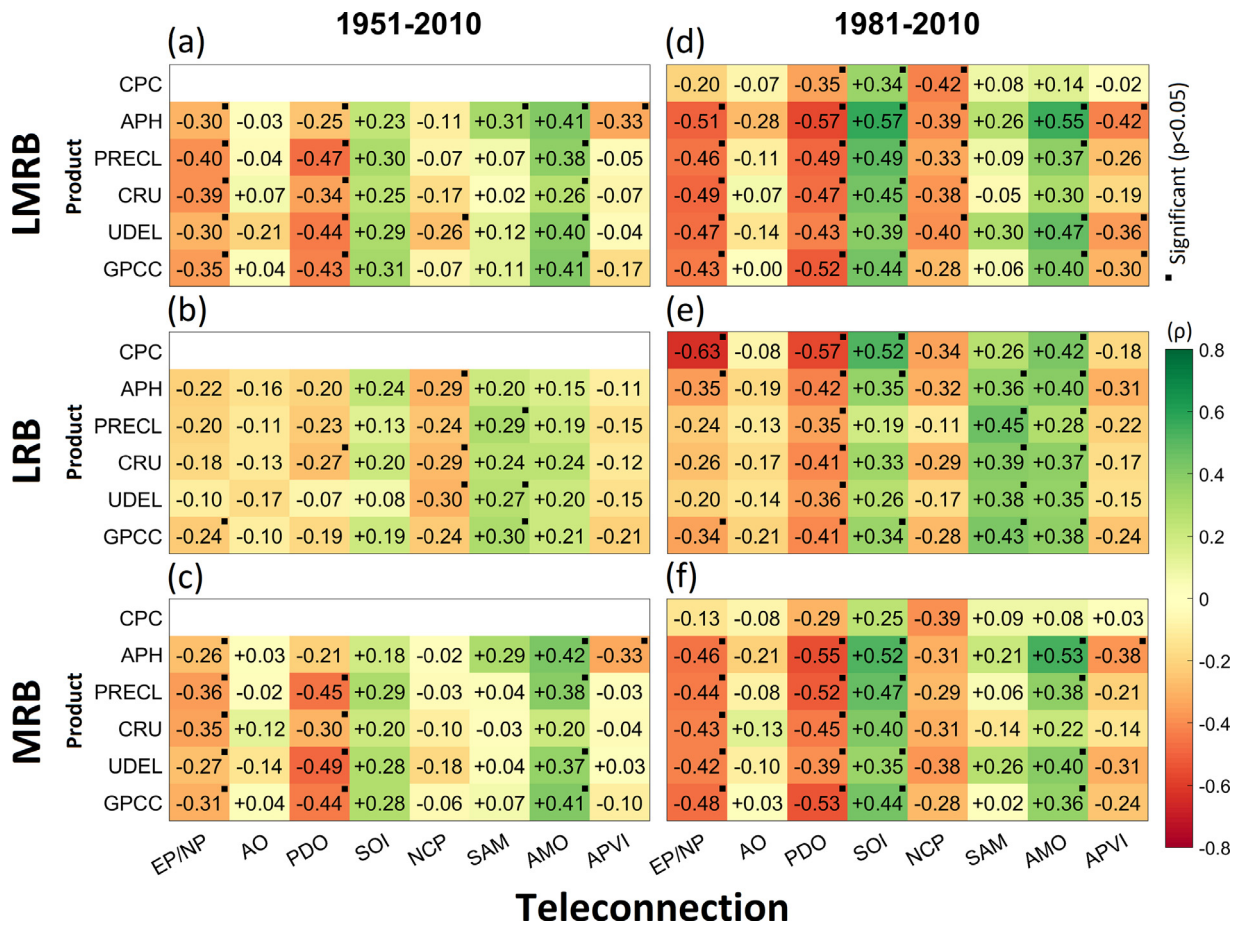
Fig. 7. The Spearman's rank correlations (ρ) of influential teleconnections with annual precipitation based on all six gauge-based gridded climate products of GPCC, UDEL, CRU, PRECL, APHRODITE (APH), and CPC over the LMRB, LRB, and MRB during 1951-2010 and 1981-2010.
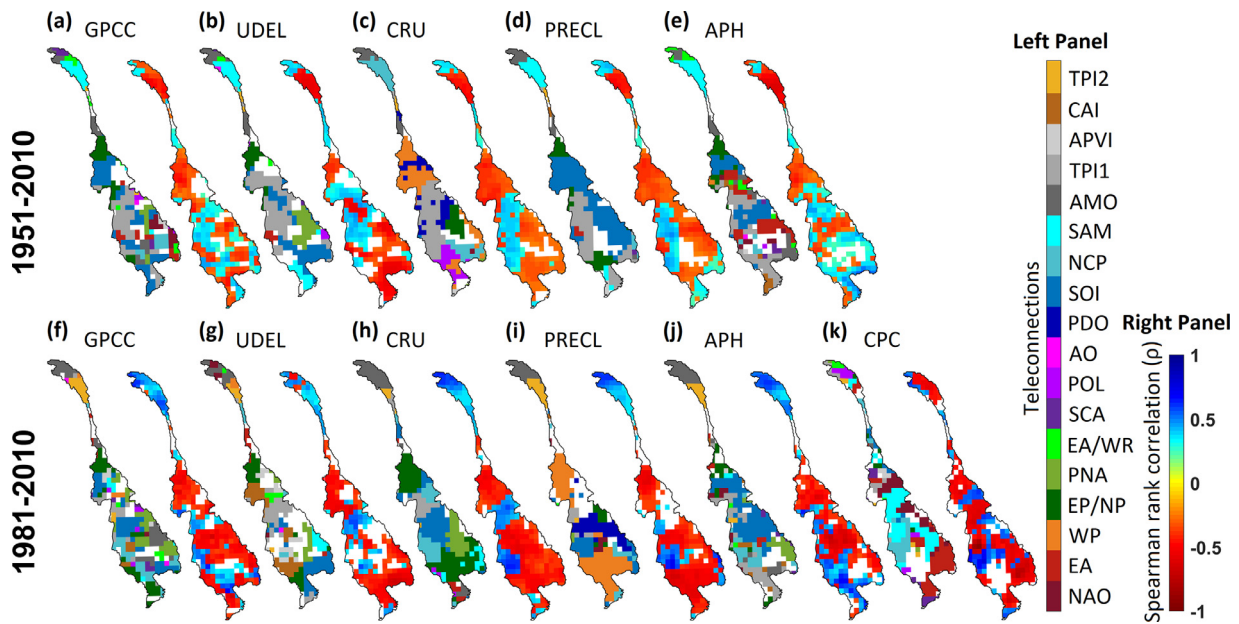
Fig. 8. The spatio-temporal pattern in the Spearman's rank correlations (ρ) of teleconnections with annual precipitation based on all six gauge-based gridded climate products of GPCC, UDEL, CRU, PRECL, APHRODITE (APH), and CPC over the LMRB during 1951-2010 and 1981-2010.
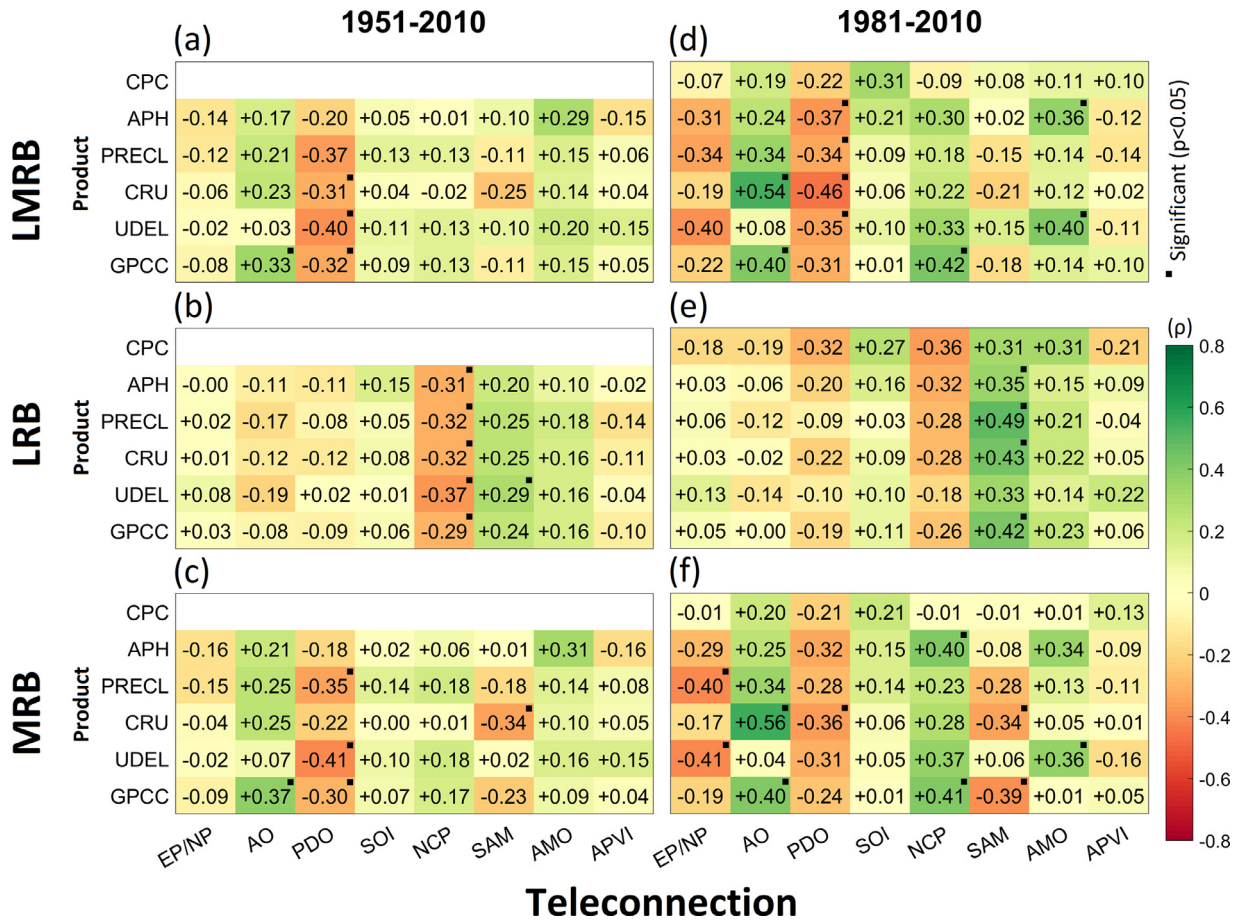
Fig. 9. The Spearman's rank correlations (ρ) of influential teleconnections with wet season precipitation based on all six gauge-based gridded climate products of GPCC, UDEL, CRU, PRECL, APHRODITE (APH), and CPC over the LMRB, LRB, and MRB during 1951-2010 and 1981-2010.
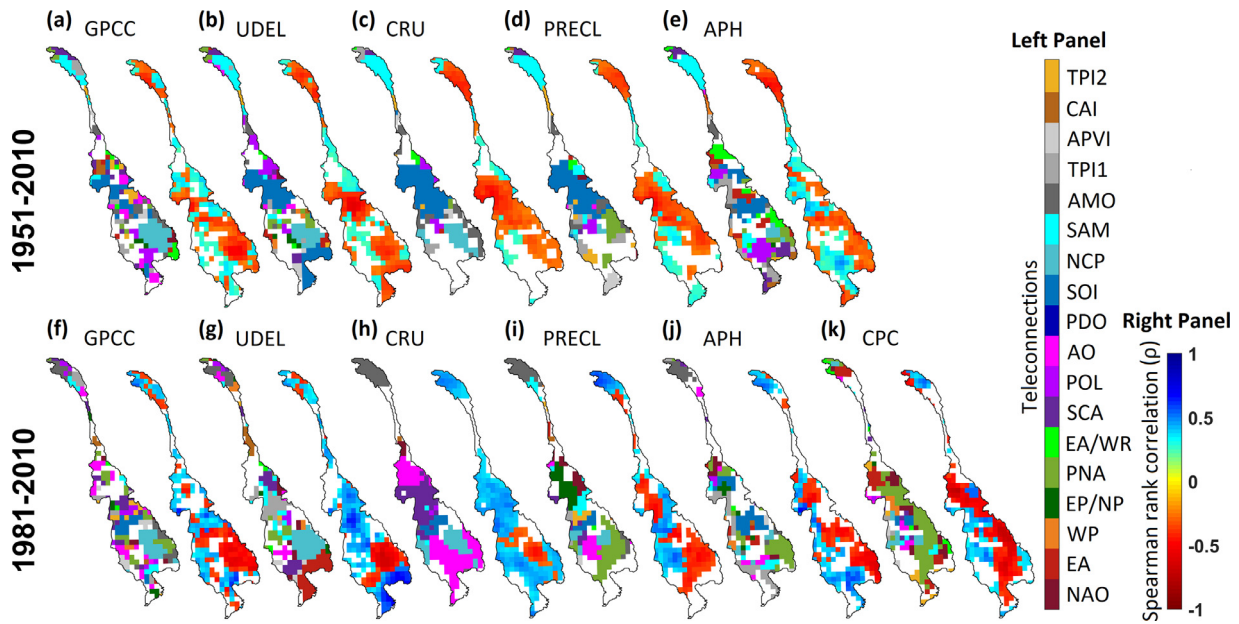
Fig. 10. The spatio-temporal pattern in the Spearman's rank correlations (ρ) of teleconnections with wet season precipitation based on all six gauge-based gridded climate products of GPCC, UDEL, CRU, PRECL, APHRODITE (APH), and CPC over the LMRB during 1951-2010 and 1981-2010.
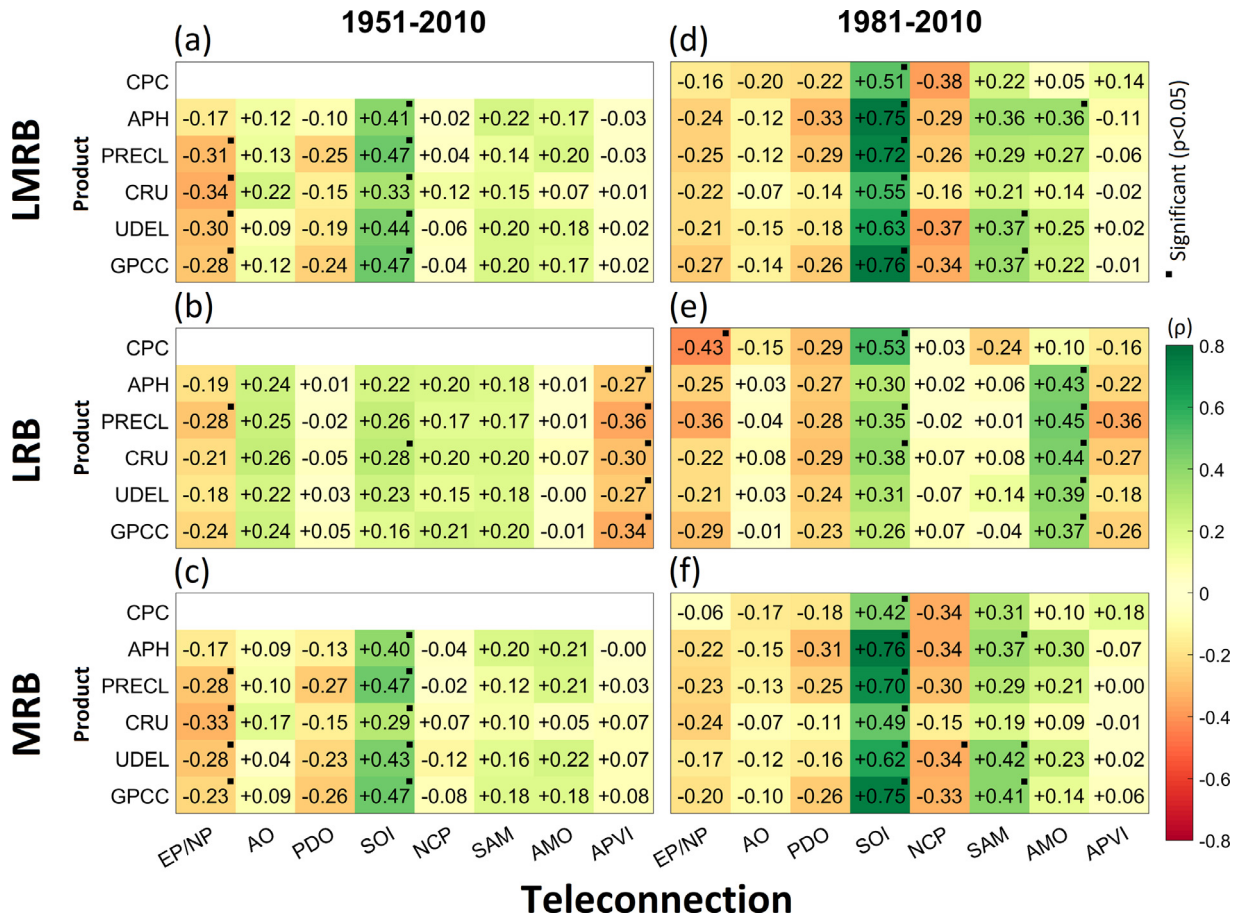
Fig. 11. The Spearman's rank correlations (*ρ*) of influential teleconnections with dry season precipitation based on all six gauge-based gridded climate products of GPCC, UDEL, CRU, PRECL, APHRODITE (APH), and CPC over the LMRB, LRB, and MRB during 1951-2010 and 1981-2010.
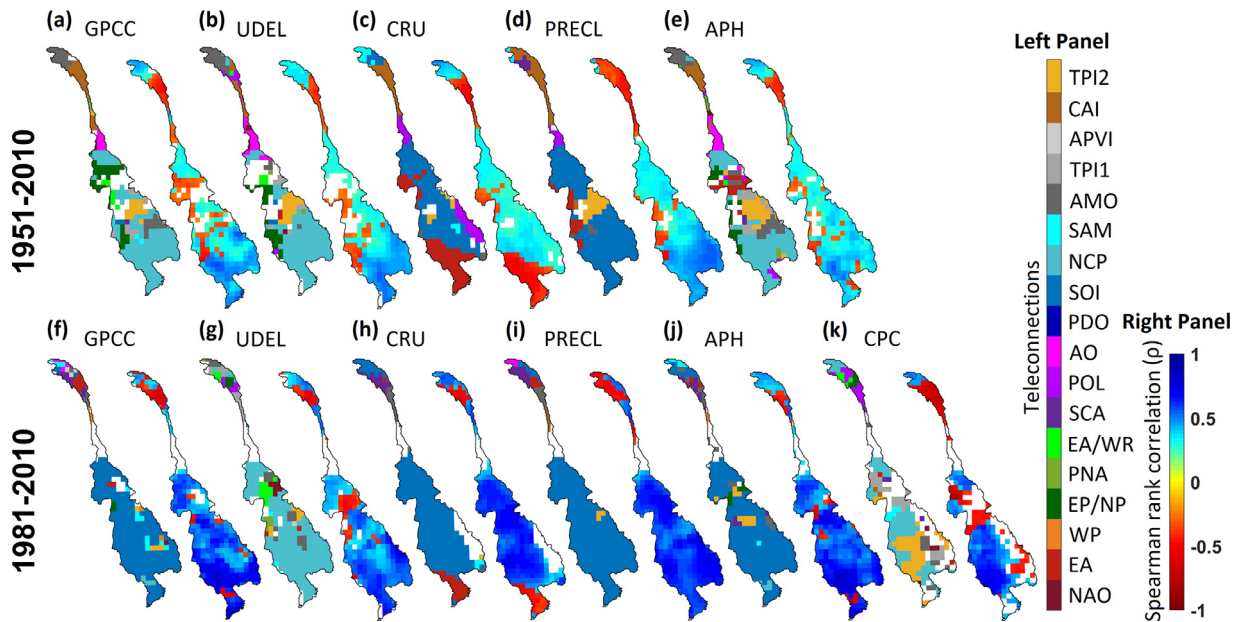
Fig. 12. The spatio-temporal pattern in the Spearman's rank correlations (*ρ*) of teleconnections with dry season precipitation based on all six gauge-based gridded climate products of GPCC, UDEL, CRU, PRECL, APHRODITE (APH), and CPC over the LMRB during 1951-2010 and 1981-2010.
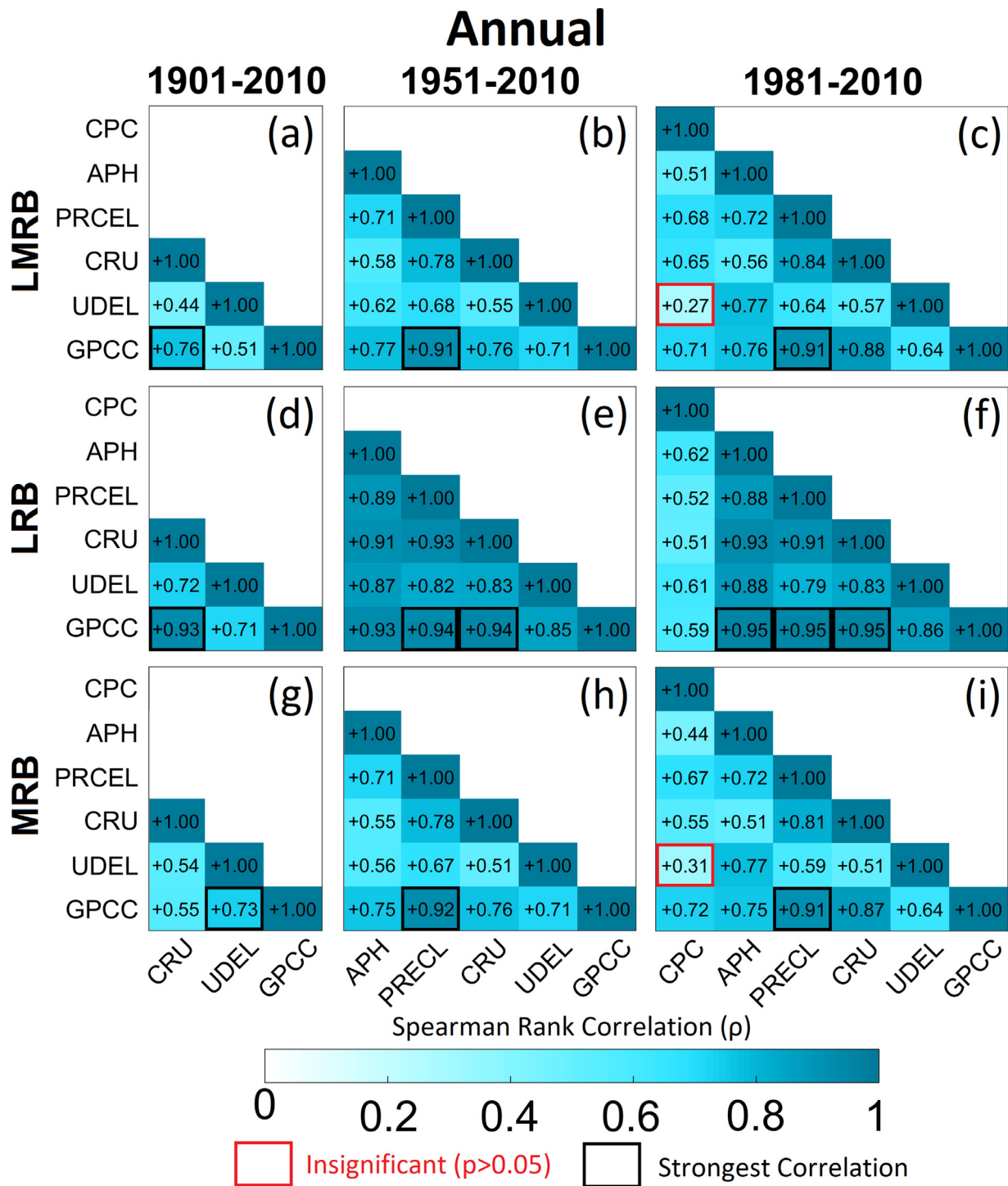
Fig. 13. The Spearman's rank correlations (ρ) among the gauge-based gridded climate products of GPCC, UDEL, CRU, PRECL, APHRODITE (APH), and CPC on the annual scale over the LMRB, LRB, and MRB during 1901-2010, 1951-2010 and 1981-2010.

3.4. Consistencies between gauge-based gridded precipitation datasets over the LMRB

For precipitation, the GPCC showed the strongest connections with other five gauge-based gridded climate products over the LMRB, LRB, and MRB on both annual and seasonal scales (Fig. 13 and 14). During 1901-2010, the GPCC showed the highest consistency with the CRU for annual and wet season precipitation over the LMRB (ρ = 0.75-0.76) and the LRB (ρ = 0.94-0.95) (Fig. 13 and 14). Across the MRB, the strongest

relationships were also found between the GPCC and the CRU for wet season precipitation (ρ = 0.74) (Fig. 14g), but between the GPCC and the UDEL for both annual (ρ = 0.73) (Fig. 13g) and dry season (ρ = 0.89) (Fig. 14p) precipitation. For the period 1951-2010, the highest correlations were generally measured between the GPCC and the PRECL for annual and seasonal precipitation over the LMRB, LRB, and MRB (Fig. 13 and 14), with ρ = 0.83-0.96; only exception refers to the dry season precipitation over the LRB with the strongest correlations between the GPCC and the APHRODITE, with ρ = 0.98 (Fig. 14n). Across all LRMB,
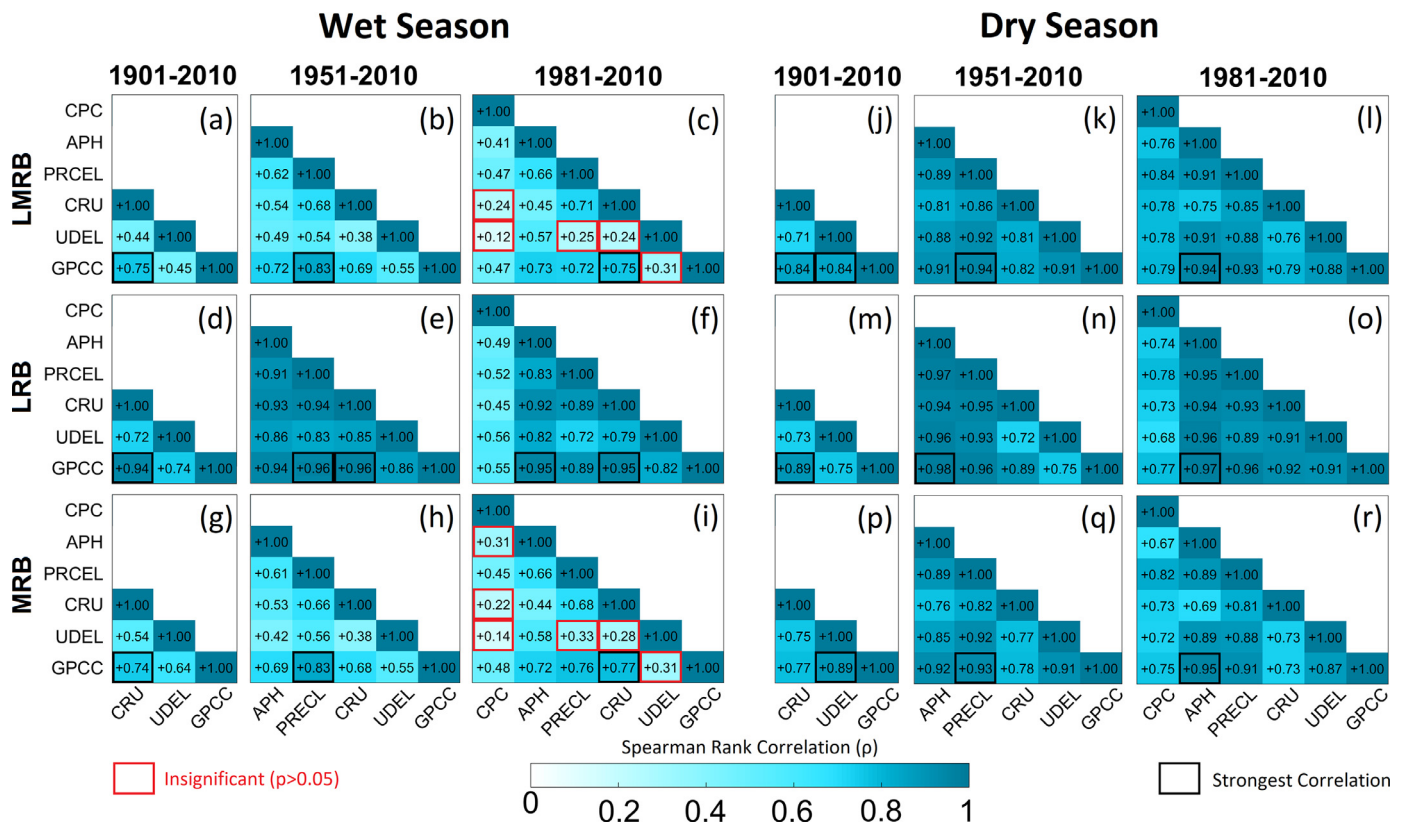
Fig. 14. The Spearman's rank correlations (ρ) among the gauge-based gridded climate products of GPCC, UDEL, CRU, PRECL, APHRODITE (APH), and CPC on the seasonal scale over the LMRB, LRB, and MRB during 1901-2010, 1951-2010 and 1981-2010.

LRB, and MRB, the highest consistencies in recent decades (1981-2010) were found between the GPCC and the PRECL for annual precipitation ($\rho = 0.91$-0.95) (Fig. 13c-f and i), the GPCC and the CRU for wet season precipitation ($\rho = 0.75$-0.95) (Fig. 14c-f and i), and the GPCC and the APHRODITE for dry season precipitation ($\rho = 0.94$-0.97) (Fig. 14l-o and r). Besides, there were other statistically significant relationships among different gauge-based gridded precipitation datasets over the LRMB, LRB, and MRB on both annual and seasonal scale, represented in Fig. 13 and 14.

On the spatial scale, the strongest century-long (1901-2010) correlations were generally measured between the GPCC and CRU over the north of LRB, the CRU and the UDEL over the south of LRB and the north of MRB, and the GPCC and the UDEL over the other parts of the MRB, for both annual and seasonal precipitations (Fig. 15). During 1951-2010, the highest consistencies for annual and seasonal precipitation were commonly found between the CRU and the PRECL over large areas of the LRMB, except its south-eastern and most southern parts in where the GPCC and the APHRODITE most strongly correlated (Fig. 16). For annual precipitation in recent decades (1981-2010), the strongest relationships were observed between the GPCC and the PRECL over the most part of the LRB and the west of MRB, while between the GPCC and the APHRODITE across the southern and western parts of MRB (Fig. 17a-f). For wet season precipitation, the highest consistencies were between the GPCC and APHRODITE throughout the east and south of the MRB during 1981-2010, the GPCC and CRU over other parts of MRB, and the CRU and PRECL over the entire LRB (Fig. 17g-l). For dry season precipitation, the strongest associations were between the GPCC and APHRODITE over the entire LRB as well as the south, east, and northeast of the MRB in 1981-2010; while the GPCC and the PRECL showed the highest consistencies across the other parts (Fig. 17m-r).

4. Discussion

In general, this paper found wetting trends in annual precipitation over the LMRB, LRB, and MRB during 1981-2010. Previous studies have also concluded such increases in annual precipitation over the LMRB (Chen et al., 2019; Delgado et al., 2010, 2012; Räsänen et al., 2012), LRB (Fan and He, 2015), and MRB (Lutz et al., 2014) in recent decades. Similar to the present paper, Fan and He (2015) reported increases in annual precipitation over the LRB during 1951-2010, and Xue et al. (2011) concluded no clear changes over the MRB. For the water years (from November to the following October) between 1952 and 2015, Irannezhad et al. (2020) also reported no statistically significant trends in annual precipitation over the LMRB, MRB, and LRB. Besides, trends in annual precipitation throughout the LMRB were inconclusive for 1901-2010. However, similar to our study, Lutz et al. (2014) reported century-long increases in the annual CRU precipitation time series over the LMRB. Wetting (drying) trends in annual precipitation were generally significant over the north and east (small areas in the south and west) of the MRB over time.

In 1981-2010, both wet and dry seasons generally got wetter over all three basins studied here. Similarly, such wetting trends in wet and dry season precipitation over the MRB and the LRB in recent decades were reported by Lutz et al. (2014) and Fan and He (2015), respectively. For the period 1951-2010, dry seasons largely showed increases in precipitation over the LMRB, LRB, and MRB, while wet seasons became drier. Such wetter dry and drier wet seasons since 1951 have previously been concluded over the LRB (Fan and He, 2015) and the MRB (Lutz et al., 2014). Irannezhad et al. (2020) also reported wetter dry seasons, but no clear trends in wet season precipitation across the LRB and MRB during 1952-2015. For 1901-2010, this study determined decreases in dry and wet season precipitation based on the UDEL dataset, while in-
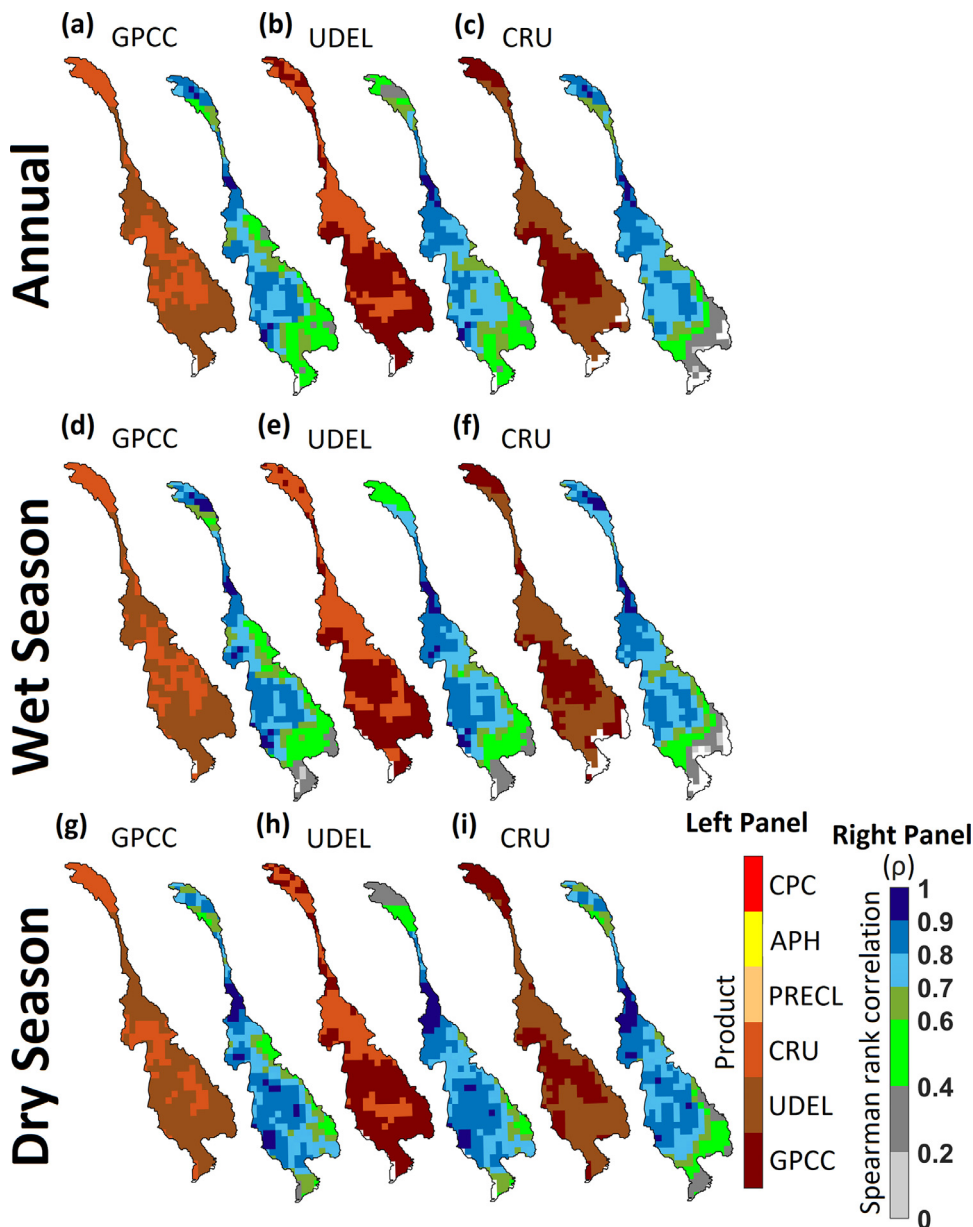
Fig. 15. The spatio-temporal pattern of consistencies among the gauge-based gridded climate products of GPCC, UDEL, CRU, PRECL, APHRODITE (APH), and CPC for estimating annual and seasonal precipitation time series over the LMRB during 1901-2010.

creases based on the CRU and the GPCC. The century-long (1901-2013) analysis of precipitation throughout the LMRB by Ruiz-Barradas and Nigam (2018) also found decreases in March-May (the three last months of the dry season) over the LRB as well as in June-November (covering wet season) across the MRB. Spatially, increases and decreases in wet season precipitation showed a similar pattern to the wetting and drying trends in annual precipitation trends. However, dry season precipitation significantly increased over the north of the LRB and the northeast and east of the MRB.

On both annual and seasonal scales, wetting and drying trends determined in precipitation were principally in association with increases in its variability across the LMRB over time. Previous studies have also reported such increases in annual and seasonal precipitation variability throughout the LMRB (e.g., Delgado et al., 2010, 2012; Lutz et al., 2014; Räsänen et al., 2012). The range of long-term average values for annual and seasonal precipitation over all three basins in 1981-2010 was generally higher than in 1951-2010 and 1901-2010. Similarly, Lutz et al. (2014) concluded higher long-term average values for both annual and seasonal precipitation over the MRB during 1981-2010, with

respect to 1941-1980 and 1901-1940. In all three basins, increases in wet season precipitation variability were basically referred to the lower (drier) long-term average values seen over time. Similarly, increases in dry season precipitation variability were principally attributed to the lower (drier) long-term average values over the LMRB and the MRB in recent decades, but to the higher (wetter) values across the LRB. On the spatial scale, long-term average values of annual and seasonal precipitation naturally increased from northwest to southeast of the LMRB, with two high centers in the lower part of the MRB, where there is a decreasing gradient from east to west. Such spatial patterns in annual and seasonal precipitation have previously been reported (e.g., Chen et al., 2018; Lutz et al., 2014).

Variations and trends in annual and seasonal precipitation throughout the LMRB over time were significantly associated with a number of teleconnections. Compared to 1951-2010, the significant correlations of these teleconnections, particularly SOI, PDO, AMO, EP/NP, and SAM, with annual and seasonal precipitation across the LMRB strengthened in 1981-2010. Such stronger relationships can partially explain wetting trends detected in both annual and seasonal precipitation time series
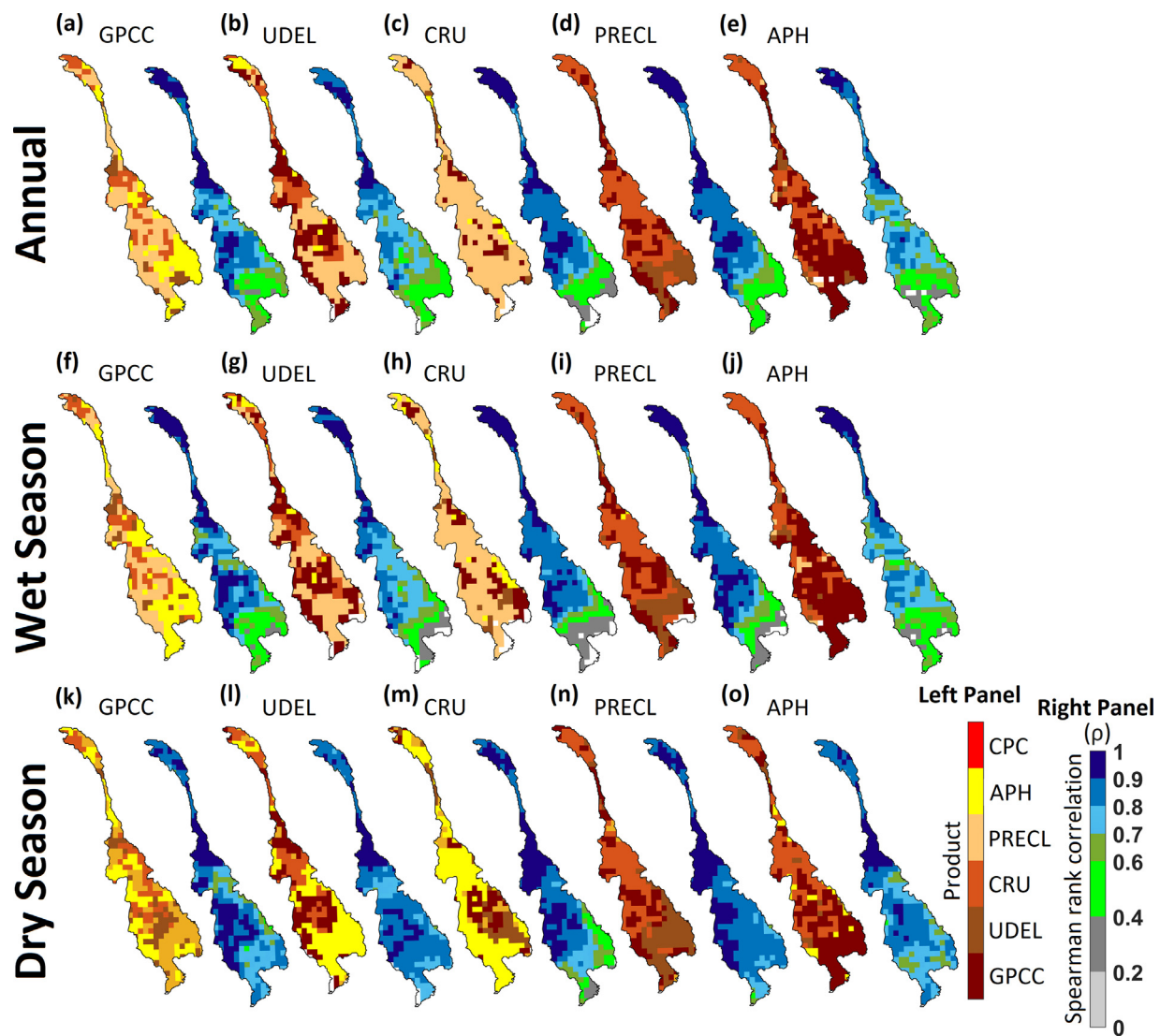
Fig. 16. The spatio-temporal pattern of consistencies among the gauge-based gridded climate products of GPCC, UDEL, CRU, PRECL, APHRODITE (APH), and CPC for estimating annual and seasonal precipitation time series over the LMRB during 1951-2010.

across the LMRB during recent decades. The stronger positive events of SOI (La Niña) naturally causes precipitation to increase throughout the Southeast Asia (e.g., Juneng and Tangang, 2005; Räsänen et al., 2016; Räsänen and Kummu, 2013; Wang et al., 2000). Such stronger positive SOI events (La Niña) are generally accompanied by the stronger negative phase of PDO, which is also associated with more precipitation across the West Pacific, covering the LMRB (Chen et al., 2019; Delgado et al., 2012; Verdon and Franks, 2006). As the AMO leads (lags) the PDO by approximately 13 (17) years in the same 60-year oscillation cycle (d'Orgeville and Peltier, 2007), its positive influence on increasing precipitation over the LMRB was stronger in 1981-2010 than in 1951-2010. Wetter climatic conditions across the LMRB during 1981-2010 were also associated with the stronger negative EP/NP events, which naturally increase precipitation over Central Vietnam and adjacent islands including Hainan (China) and the Philippines (Li et al., 2015). Besides, wetter wet seasons over the LRB in 1981-2010 showed the most robust associations with the positive SAM events, which shift westerlies towards the Antarctic and thereby supports stronger positive SOI events (La Niña) with higher precipitation over the mainland Southeast Asia.

This paper measured consistencies among different gauge-based gridded climate products created based on in-situ precipitation records throughout the LMRB in three study periods of 1901-2010, 1951-2010, and 1981-2010. Such relationships generally strengthened over time. This may mainly refer to the application of more and/or similar in-situ records in recent decades for generating these products. Spatially, the strongest and weakest consistencies were found over the LRB and the MRB, respectively, for both annual and seasonal precipitation. This is principally because of the lower number of stations available as well as the substantially lower amounts of annual and seasonal precipitation in the LRB than in the MRB. Based on the time resolution, the gauge-based gridded climate products were most significantly consistent in generating the dry season precipitation time series throughout the LMRB, LRB, and MRB. This is mainly due to the lower range of precipitation during the dry than wet season across all three basins. Previous studies also reported that consistencies among the gauge-based gridded climate products are largely dependent on the number of similar/different precipitation measurement stations used, the climate of study area, the time resolution, the manner of analysis, the procedure of quality control, and the study period (e.g., Hegerl et al., 2015; Sun et al., 2014, 2018). Accordingly, this paper concluded that GPCC is most strongly associated with other products on both annual and seasonal scales over all three basins and study periods. This product (GPCC) was previously
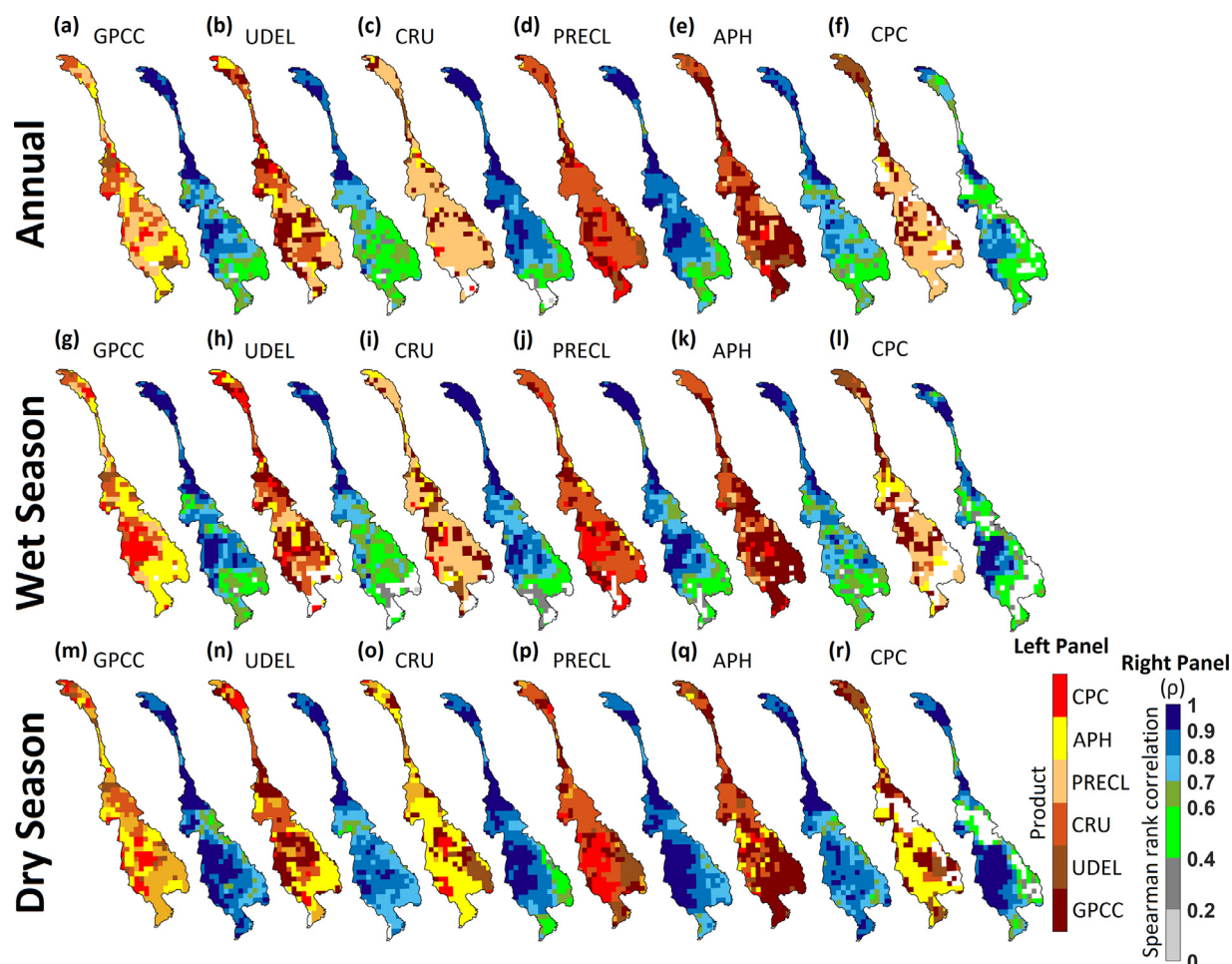
Fig. 17. The spatio-temporal pattern of consistencies among the gauge-based gridded climate products of GPCC, UDEL, CRU, PRECL, APHRODITE (APH), and CPC for estimating annual and seasonal precipitation time series over the LMRB during 1981-2010.

used by Sun et al. (2018) as the reference to examine the reliability of other gauge-based gridded climate products (including UDEL, CRU, PRECL, and CPC) for analyzing precipitation patterns on both regional and global scales. Yatagai et al. (2012) also confirmed the accuracy and reliability of APHRODITE based on the GPCC product. Similar to Yatagai et al. (2012), this study used daily APHRODITE datasets to calculate its annual and seasonal scale, which showed significant relationships with corresponding GPCC datasets computed from the monthly scale. After GPCC, PRECL and then APHRODITE showed the highest consistencies with other products for studying precipitation variability and trends throughout the LMRB.

5. Conclusions

This study provided a detailed overview of historical precipitation patterns over the Lancang-Mekong River Basin (LMRB) utilizing six gauge-based gridded climate products of GPCC, UDEL, CRU, PRECL, APHRODITE, and CPC. Accordingly, the present paper evaluated long-term trends, variability, consistency, and links to teleconnections for annual and seasonal (wet and dry) precipitation throughout the LMRB during 1901-2010, 1951-2010, and 1981-2010. Annual and seasonal precipitation amounts naturally increase from northwest to southeast of the LMRB, but with a spatial gradient increasing from west to east throughout the lower parts of the Mekong River Basin (MRB). The LMRB, Lancang River Basin (LRB), and MRB experienced increases in annual precipitation during 1951-2010 and 1981-2010. The dry (wet) seasons got wetter (drier) in 1951-2010, while both dry and wet seasons got wetter

during 1981-2010. Such changes in annual and dry (wet) season precipitation over all three basins (LRB) were most significantly associated with the SOI (SAM), which strengthened during 1981-2010. Hence, wetting trends in annual and wet (dry) season precipitation were mostly found across the north and east of the MRB (the northern parts of the LRB as well as the northeast and east of the MRB). Such historical precipitation trends, variability, and links to teleconnections over the LMRB were identical among different gauge-based gridded climate products, with the strongest (weakest) consistencies throughout the north of LRB (the south and southeast of the MRB) due to relatively drier (wetter) climatic conditions. Accordingly, GPCC (APHRODITE) can be applied as the primary gauge-based gridded climate product for further studies on the effects of climate variability and change on water resources in the LMRB before (after) 1951. In particular, the APHRODITE product is suggested as the key source of dry season precipitation dataset across all the LMRB, LRB, and MRB for the period 1951-2010.

Data Availability

All datasets analyzed during this study are publicly available through the references given in the manuscript.

Declaration of Competing Interest

The authors declare that they have no known competing financial interests or personal relationships that could have appeared to influence the work reported in this paper.

Acknowledgments

Supplementary materials

Supplementary material associated with this article can be found, in the online version, at doi:10.1016/j.geosus.2022.03.002.

References

AghaKouchak, A., Chiang, F., Huning, L.S., Love, C.A., Mallakpour, I., Mazdiyasni, O., Moftakhari, H., Papalexiou, S.M., Ragno, E., Sadegh, M., 2020. Climate extremes and compound hazards in a warming world. Annu. Rev. Earth Planet. Sci. 48, 519–548.

Andersson, E., Bauer, P., Beljaars, A., Chevallier, F., Hólm, E., Janisková, M., Kallberg, P., Kelly, G., Lopez, P., McNally, A., Moreau, E., Simmons, A.J., Thépaut, J.-N., Tompkins, A.M., 2005. Assimilation and modeling of the atmospheric hydrological cycle in the ECMWF forecasting system. Bull. Am. Meteorol. Soc. 96 (3), 387–402.

Barnston, A.G., Livezey, R.E., 1987. Classification, seasonality and persistence of low-frequency atmospheric circulation patterns. Mon. Weather Rev. 115 (6), 1083–1126.

Berghuijs, W.R., Larsen, J.R., van Emmerik, T.H.M., Woods, R.A., 2017. A global assessment of runoff sensitivity to changes in precipitation, potential evaporation, and other factors. Water Resour. Res. 53 (10), 8475–8486.

Bueh, C., Nakamura, H., 2007. Scandinavian pattern and its climatic impact. Q. J. R. Meteorol. Soc. 133 (629 B), 2117–2131.

Chen, A., Chen, D., Azorin-Molina, C., 2018. Assessing reliability of precipitation data over the Mekong River Basin: A comparison of ground-based, satellite, and reanalysis datasets. Int. J. Climatol. 38 (11), 4314–4334.

Chen, A., Ho, C.-H., Chen, D., Azorin-Molina, C., 2019. Tropical cyclone rainfall in the Mekong River Basin for 1983–2016. Atmos. Res. 226, 66–75.

Chen, M., Xie, P., Janowiak, J.E., Arkin, P.A., 2002. Global land precipitation: A 50-yr monthly analysis based on gauge observations. J. Hydrometeorol. 3 (3), 249–266.

d'Orgeville, M., Peltier, W.R., 2007. On the Pacific decadal oscillation and the Atlantic multidecadal oscillation: Might they be related? Geophys. Res. Lett. 34 (23), L23705.

Deininger, M., McDermott, F., Cruz, F.W., Bernal, J.P., Mudelsee, M., Vonhof, H., Millo, C., Spötl, C., Treble, P.C., Pickering, R., Scholz, D., 2020. Inter-hemispheric synchroneity of Holocene precipitation anomalies controlled by Earth's latitudinal insolation gradients. Nat. Commun. 11 (1), 5447.

Delgado, J.M., Apel, H., Merz, B., 2010. Flood trends and variability in the Mekong River. Hydrol. Earth Syst. Sci. 14 (3), 407–418.

Delgado, J.M., Merz, B., Apel, H., 2012. A climate-flood link for the lower Mekong River. Hydrol. Earth Syst. Sci. 16 (5), 1533–1541.

Enfield, D.B., Mestas-Nuñez, A.M., Trimble, P.J., 2001. The Atlantic multidecadal oscillation and its relation to rainfall and river flows in the continental U.S. Geophys. Res. Lett. 28 (10), 2077–2080.

Fan, H., He, D., 2015. Temperature and precipitation variability and its effects on streamflow in the upstream regions of the Lancang-Mekong and Nu-Salween Rivers. J. Hydrometeorol. 16 (5), 2248–2263.

Ghasemifar, E., Irannezhad, M., Minaei, F., Minaei, M., 2022. The role of ENSO in atmospheric water vapor variability during cold months over Iran. Theor. Appl. Climatol. doi:10.1007/s00704-022-03969-x.

Glantz, M.H., Katz, R.W., Nicholls, N., 2009. Teleconnections Linking Worldwide Climate Anomalies : Scientific Basis and Societal Impact. Cambridge University Press, Cambridge.

Groisman, P.Y., Legates, D.R., 1995. Documenting and detecting long-term precipitation trends: Where we are and what should be done. Clim. Change 31 (2–4), 601–622.

Gudmundsson, L., Boulange, J., Do, H.X., Gosling, S.N., Grillakis, M.G., Koutroulis, A.G., Leonard, M., Liu, J., Schmied, H.M., Papadimitriou, L., Pokhrel, Y., Seneviratne, S.I., Satoh, Y., Thiery, W., Westra, S., Zhang, X., Zhao, F., 2021. Globally observed trends in mean and extreme river flow attributed to climate change. Science 371 (6534), 1159–1162.

Gupta, A., Hock, L., Xiaojing, H., Ping, C., 2002. Evaluation of part of the Mekong River using satellite imagery. Geomorphology 44 (3-4), 221–239.

Harris, I., Jones, P.D., Osborn, T.J., Lister, D.H., 2014. Updated high-resolution grids of monthly climatic observations - the CRU TS3.10 Dataset. Int. J. Climatol. 34 (3), 623–642.

Hegerl, G.C., Black, E., Allan, R.P., Ingram, W.J., Polson, D., Trenberth, K.E., Chadwick, R.S., Arkin, P.A., Sarojini, B.B., Becker, A., Dai, A., Durack, P.J., Easterling, D., Fowler, H.J., Kendon, E.J., Huffman, G.J., Liu, C., Marsh, R., New, M., Osborn, T.J., Skliris, N., Stott, P.A., Vidale, P.-L., Wijffels, S.E., Wilcox, L.J., Willett, K.M., Zhang, X., 2015. Challenges in quantifying changes in the global water cycle. Bull. Am. Meteorol. Soc. 96 (7), 1097–1115.

Helsel, D.R., Hirsch, R.M., 1992. Statistical methods in water resources. U.S. Geological Survey, Reston.

Houghton, J., Townshend, J., Dawson, K., Mason, P., Zillman, J., Simmons, A., 2012. The GCOS at 20 years: The origin, achievement and future development of the Global Climate Observing System. Weather 67 (9), 227–235.

Hrudya, P.H., Varikoden, H., Vishnu, R., 2021. A review on the Indian summer monsoon rainfall, variability and its association with ENSO and IOD. Meteorol. Atmos. Phys. 133, 1–14.

Hugelius, G., Loisel, J., Chadburn, S., Jackson, R.B., Jones, M., MacDonald, G., Marushchak, M., Olefeldt, D., Packalen, M., Siewert, M.B., Treat, C., Turetsky, M., Voigt, C., Yu, Z., 2020. Large stocks of peatland carbon and nitrogen are vulnerable to permafrost thaw. Proc. Natl. Acad. Sci. U.S.A. 117 (34), 20438–20446.

IPCC, 2021. Climate Change 2021: The Physical Science Basis. Contribution of Working Group I to the Sixth Assessment Report of the Intergovernmental Panel on Climate Change. Cambridge University Press. In Press [Masson-Delmotte, V., P. Zhai, A. Pirani, S.L. Connors, C. Péan, S. Berger, N. Caud, Y. Chen, L. Goldfarb, M.I. Gomis, M. Huang, K. Leitzell, E. Lonnoy, J.B.R. Matthews, T.K. Maycock, T. Waterfield, O. Yelekçi, R. Yu, and B. Zhou (eds.)].

Irannezhad, M., Ahmadi, B., Liu, J., Chen, D., Matthews, J.H., 2022. Global water security: A shining star in the dark sky of achieving the sustainable development goals. Sustain. Horizons 1, 100005.

Irannezhad, M., Liu, J., Chen, D., 2020. Influential climate teleconnections for spatiotemporal precipitation variability in the Lancang-Mekong River Basin from 1952 to 2015. J. Geophys. Res. Atmos. 125 (21), e2020JD033331.

Irannezhad, M., Liu, J., Chen, D., 2021. Extreme precipitation variability across the Lancang-Mekong River Basin during 1952-2015 in relation to teleconnections and summer monsoons. Int. J. Climatol. doi:10.1002/joc.7370.

Irannezhad, M., Marttila, H., Kløve, B., 2014. Long-term variations and trends in precipitation in Finland. Int. J. Climatol. 34 (10), 3139–31553.

Irannezhad, M., Minaei, M., Ahmadian, S., Chen, D., 2018. Impacts of changes in climate and land cover-land use on flood characteristics in Gorganrood Watershed (Northeastern Iran) during recent decades. Geogr. Ann. A.: Phys. Geogr. 100 (4), 340–350.

Iz, H.B., 2018. Is the global sea surface temperature rise accelerating? Geod. Geodyn. 9 (6), 432–438.

Jacobs, J.W., 2002. The Mekong River Commission: Transboundary water resources planning and regional security. Geogr. J. 168 (4), 354–364.

Jiang, S., Ren, L., Hong, Y., Yong, B., Yang, X., Yuan, F., Ma, M., 2012. Comprehensive evaluation of multi-satellite precipitation products with a dense rain gauge network and optimally merging their simulated hydrological flows using the Bayesian model averaging method. J. Hydrol. 452-453, 213–225.

Jiang, Z., Jiang, S., Shi, Y., Liu, Z., Li, W., Li, L., 2017. Impact of moisture source variation on decadal-scale changes of precipitation in North China from 1951 to 2010. J. Geophys. Res. Atmos. 122 (2), 600–613.

Jones, P.D., Salinger, M.J., Mullan, A.B., 1999. Extratropical circulation indices in the Southern Hemisphere based on station data. Int. J. Climatol. 10 (12), 1301–1317.

Juneng, L., Tangang, F.T., 2005. Evolution of ENSO-related rainfall anomalies in Southeast Asia region and its relationship with atmosphere - Ocean variations in Indo-Pacific sector. Clim. Dyn. 25 (4), 337–350.

Kidd, C., Becker, A., Huffman, G.J., Muller, C.L., Joe, P., Skofronick-Jackson, G., Kirschbaum, D.B., 2017. So, how much of the Earth's surface is covered by rain gauges? Bull. Am. Meteorol. Soc. 98 (1), 69–78.

Konapala, G., Mishra, A.K., Wada, Y., Mann, M.E., 2020. Climate change will affect global water availability through compounding changes in seasonal precipitation and evaporation. Nat. Commun. 11 (1), 3044.

Kutiel, H., Benaroch, Y., 2002. North Sea-Caspian pattern (NCP) - An upper level atmospheric teleconnection affecting the Eastern Mediterranean: Identification and definition. Theor. Appl. Climatol. 71 (1-2), 17–28.

Li, R., Wang, S.Y., Gillies, R.R., Buckley, B.M., Truong, L.H., Cho, C., 2015. Decadal oscillation of autumn precipitation in Central Vietnam modulated by the East Pacific-North Pacific (EP-NP) teleconnection. Environ. Res. Lett. 10 (2), 024008.

Lim, Y.K., Kim, H.D., 2013. Impact of the dominant large-scale teleconnections on winter temperature variability over East Asia. J. Geophys. Res. Atmos. 118 (14), 7835–7848.

Liu, A., Soneja, S.I., Jiang, C., Huang, C., Kerns, T., Beck, K., Mitchell, C., Sapkota, A., 2017a. Frequency of extreme weather events and increased risk of motor vehicle collision in Maryland. Sci. Total Environ. 580, 550–555.

Liu, J., Bawa, K.S., Seager, T.P., Mao, G., Ding, D., Lee, J.S.H., Swim, J.K., 2019. On knowledge generation and use for sustainability. Nat. Sustain. 2 (2), 80–82.

Zhao, Y., Wu, F., Li, F., Chen, X.-N., Xu, X., Shao, Z.-Y., 2021. Ecological compensation standard of trans-boundary river basin based on ecological spillover value: A case study for the Lancang–Mekong River Basin. Int. J. Environ. Res. Public Health 18 (3), 1251.

Zhu, Y., Sang, Y.-F., Chen, D., Sivakumar, B., Li, D., 2020. Effects of the South Asian summer monsoon anomaly on interannual variations in precipitation over the South–Central Tibetan Plateau. Environ. Res. Lett. 15, 124067.

Liu, J., Chen, D., Mao, G., Irannezhad, M., Pokhrel, Y., 2021a. Past and future changes in climate and water resources in the LancangMekong River Basin: Current understanding and future research directions. Engineering. doi:10.1016/j.eng.2021.06.026.

Liu, X., Yang, T., Hsu, K., Liu, C., Sorooshian, S., 2017b. Evaluating the streamflow simulation capability of PERSIANN-CDR daily rainfall products in two river basins on the Tibetan Plateau. Hydrol. Earth Syst. Sci. 21 (1), 169–181.

Liu, Y., Zhang, C., Tang, Q., Hosseini-Moghari, S.M., Haile, G.G., Li, L., Li, W., Yang, K., van der Ent, R.J., Chen, D., 2021b. Moisture source variations for summer rainfall in different intensity classes over Huaihe River Valley. China. Clim. Dyn. 57 (3-4), 1121–1133.

Mann, H.B., 1945. Non-parametric test against trend. Econometrica 13, 245.

Marshall, G.J., 2003. Trends in the Southern Annular Mode from observations and reanalyses. J. Clim. 16 (24), 4134–4143.

MRC, 2019. State of the Basin Report 2018. Mekong River Commission, Vientiane.

MRC, 2010. State of the Basin Report 2010. Mekong River Commission, Vientiane.

MRC, 2005. Overview of the Hydrology of the Mekong Basin. Mekong River Commission, Vientiane.

Lutz, A., Terink, W., Droogers, P., Immerzeel, W.W., Piman, T., 2014. Development of baseline climate data set and trend analysis in the Mekong Basin. FutureWater Report. https://doi.org/10.1175/BAMS-88-9-1383.

New, M., Hulme, M., Jones, P., 2000. Representing twentieth-century space-time climate variability. Part II: Development of 1901-96 monthly grids of terrestrial surface climate. J. Clim. 13 (13), 2217–2238.

New, M., Todd, M., Hulme, M., Jones, P., 2001. Precipitation measurements and trends in the twentieth century. Int. J. Climatol. 21 (15), 1889–1922.

Park, E., Lee, Y.J., 2001. Estimates of standard deviation of spearman's rank correlation coefficients with dependent observations. Commun. Stat. Part B: Simul. Comput. 30 (1), 129–142.

Pascale, S., Lucarini, V., Feng, X., Porporato, A., Hasson, S., 2015. Analysis of rainfall seasonality from observations and climate models. Clim. Dyn. 44 (11-12), 3281–3301.

Pathak, A., Ghosh, S., Martinez, J.A., Dominguez, F., Kumar, P., 2017. Role of oceanic and land moisture sources and transport in the seasonal and interannual variability of summer monsoon in India. J. Clim. 30 (5), 1839–1859.

Pokhrel, Y., Felfelani, F., Satoh, Y., Boulange, J., Burek, P., Gädeke, A., Gerten, D., Gosling, S.N., Grillakis, M., Gudmundsson, L., Hanasaki, N., Kim, H., Koutroulis, A., Liu, J., Papadimitriou, L., Schewe, J., Müller Schmied, H., Stacke, T., Telteu, C.-E., Thiery, W., Veldkamp, T., Zhao, F., Wada, Y., 2021. Global terrestrial water storage and drought severity under climate change. Nat. Clim. Change 11 (3), 226–233.

Radinović, D., Ćurić, M., 2009. Deficit and surplus of precipitation as a continuous function of time. Theor. Appl. Climatol. 98 (1-2), 197–200.

Räsänen, T.A., Koponen, J., Lauri, H., Kummu, M., 2012. Downstream hydrological impacts of hydropower development in the Upper Mekong Basin. Water Resour. Manag. 26 (12), 3495–3513.

Räsänen, T.A., Kummu, M., 2013. Spatiotemporal influences of ENSO on precipitation and flood pulse in the Mekong River Basin. J. Hydrol. 476, 154–168.

Räsänen, T.A., Lindgren, V., Guillaume, J.H.A., Buckley, B.M., Kummu, M., 2016. On the spatial and temporal variability of ENSO precipitation and drought teleconnection in mainland Southeast Asia. Clim. Past. 12 (9), 1889–1905.

NCC, 2019. National Climate Center of China Meteorological Administration (CMA). http://cmdp.ncc-cma.net/cn/download.htm (accessed 4 August 2019).

Rudolf, B., Becker, A., Schneider, U., Meyer-Christoffer, A., Ziese, M., 2009. The new "GPCC Full Data Reanalysis Version 5" providing high quality gridded monthly precipitation data for the global land-surface is public available since December 2010. Global Precipitation Climatology Centre Status Report.

Ruiz-Barradas, A., Nigam, S., 2018. Hydroclimate variability and change over the Mekong River Basin: Modeling and predictability and policy implications. J. Hydrometeorol. 19 (5), 849–869.

Sachs, J., Schmidt-Traub, G., Kroll, C., Durand-Delacre, D., Teksoz, K., 2017. SDG Index and Dashboards Report 2017. Bertelsmann Stiftung and Sustainable Development Solutions Network (SDSN), New York.

Sarojini, B.B., Stott, P.A., Black, E., 2016. Detection and attribution of human influence on regional precipitation. Nat. Clim. Change 6 (7), 669–675.

Schneider, U., Becker, A., Finger, P., Meyer-Christoffer, A., Ziese, M., Rudolf, B., 2014. GPCC's new land surface precipitation climatology based on quality-controlled in situ data and its role in quantifying the global water cycle. Theor. Appl. Climatol. 115 (1-2), 15–40.

Sen, P.K., 1968. Estimates of the regression coefficient based on Kendall's. Tau. J. Am. Stat. Assoc. 63 (324), 1379–1389.

Spence, T., Townshend, J., 1995. The global climate observing system (GCOS). Clim. Change 31, 131–134.

Strangeways, I., 2006. Precipitation: Theory, Measurement and Distribution. Cambridge University Press, Cambridge.

Sun, Q., Miao, C., Duan, Q., Ashouri, H., Sorooshian, S., Hsu, K.-L., 2018. A review of global precipitation data sets: Data sources, estimation, and intercomparisons. Rev. Geophys. 56 (1), 79–107.

Sun, Q., Miao, C., Duan, Q., Kong, D., Ye, A., Di, Z., Gong, W., 2014. Would the 'real' observed dataset stand up? A critical examination of eight observed gridded climate datasets for China. Environ. Res. Lett. 9 (1), 015001.

Thompson, D.W.J., Wallace, J.M., 1998. The Arctic oscillation signature in the wintertime geopotential height and temperature fields. Geophys. Res. Lett. 25 (9), 1297–1300.

Trenberth, K.E., 1984. Signal versus noise in the Southern Oscillation. Mon. Weather Rev. 112 (2), 326–332.

UN, 2015. Transforming our world: The 2030 agenda for Sustainable Development. United Nations, New York.

Verdon, D.C., Franks, S.W., 2006. Long-term behaviour of ENSO: Interactions with the PDO over the past 400 years inferred from paleoclimate records. Geophys. Res. Lett. 33 (6), L06712.

Wallace, J.M., Gutzler, D.S., 1981. Teleconnections in the geopotential height field during the Northern Hemisphere winter. Mon. Weather Rev. 109 (4), 784–812.

Wang, B., Wu, R., Fu, X., 2000. Pacific-East Asian teleconnection: How does ENSO affect East Asian climate? J. Clim. 13 (9), 1517–1536.

Wang, F., Ge, Q., Chen, D., Luterbacher, J., Tokarska, K.B., Hao, Z., 2018. Global and regional climate responses to national-committed emission reductions under the Paris agreement. Geogr. Ann. Ser. A, Phys. Geogr. 100, 240–253.

Wang, W., Lu, H., Yang, D., Sothea, K., Jiao, Y., Gao, B., Peng, X., Pang, Z., 2016. Modelling hydrologic processes in the Mekong River basin using a distributed model driven by satellite precipitation and rain gauge observations. PLoS One 11 (3), e0152229.

Ward, P.J., Beets, W., Bouwer, L.M., Aerts, J.C.J.H., Renssen, H., 2010. Sensitivity of river discharge to ENSO. Geophys. Res. Lett. 37 (12), L12402.

Willmott, C.J., Matsuura, K., 1995. Smart interpolation of annually averaged air temperature in the United States. J. Appl. Meteorol. 34 (12), 2577–2586.

Xie, P., Chen, M., Shi, W., 2010. CPC global unified gauge-based analysis of daily precipitation. In: 24th Conference on Hydrology. Amer. Meteor. Soc, Atlanta, GA, p. 2.

Xue, Z., Liu, J.P., Ge, Q., 2011. Changes in hydrology and sediment delivery of the Mekong River in the last 50 years: Connection to damming, monsoon, and ENSO. Earth Surf. Process. Landf. 36, 296–308.

Yang, R., Zhang, W.K., Gui, S., Tao, Y., Cao, J., 2019. Rainy season precipitation variation in the Mekong River basin and its relationship to the Indian and East Asian summer monsoons. Clim. Dyn. 52, 5691–5708.

Yatagai, A., Arakawa, O., Kamiguchi, K., Kawamoto, H., Nodzu, M.I., Hamada, A., 2009. A 44-year daily gridded precipitation dataset for Asia based on a dense network of rain gauges. Sci. Online Lett. Atmosphere 5, 137–140.

Yatagai, A., Kamiguchi, K., Arakawa, O., Hamada, A., Yasutomi, N., Kitoh, A., 2012. Aphrodite constructing a long-term daily gridded precipitation dataset for Asia based on a dense network of rain gauges. Bull. Am. Meteorol. Soc. 93, 1401–1415.

Yin, J., Yin, Z., Zhong, H., Xu, S., Hu, X., Wang, J., Wu, J., 2011. Monitoring urban expansion and land use/land cover changes of Shanghai metropolitan area during the transitional economy (1979–2009) in China. Environ. Monit. Assess. 177, 609–621.

Yue, S., Pilon, P., Phinney, B., Cavadias, G., 2002. The influence of autocorrelation on the ability to detect trend in hydrological series. Hydrol. Process. 16, 1807–1829.

Zhang, R.H., Levitus, S., 1997. Structure and cycle of decadal variability of upper-ocean temperature in the North Pacific. J. Clim. 10, 710–727.